Measuring the Pulse Duration and the Time-Dependent Polarisation State of Ultrashort Laser Pulses with the D-Scan Technique

MASTER THESIS

by Daniel Díaz Rivas

Abstract

Ultrashort laser pulses with time-dependent polarisation states have many applications, such as the generation of isolated attosecond pulses and the study of the optical chirality of molecules. In this project the polarisation gate, built from two quarter-wave plates of different orders, is thoroughly characterised in experiment and simulation. The time-dependent polarisation state is investigated with the dispersion scan technique (d-scan). We demonstrate that it is sufficient to measure three different projections of the electric field with the d-scan in order to achieve its complete reconstruction.

Acknowledgments

I would like to start by expressing my gratitude to Cord, without whom I would have not found this project in the first place. As director of the master, teacher and thesis supervisor you have been a constant source of guidance and support since I came to Lund two years ago. I can not thank enough my co-supervisor Ann-Kathrin, who has dedicated so many hours to help me during the thesis. You have made this work much more valuable.

Thank you Chen for always being available to help me. Your expertise in optics has helped me understand countless things about d-scan, simulations, etc. Thank you Anne-Lise, Ivan, Serhii, Venus and Lucas for spending so much time in the office and in the lab and making me feel very comfortable working. Thanks to all the colleagues in the Division of Atomic Physics, who have supported me and with whom I share many happy memories.

I want to especially thank my two classmates in the Photonics Master programme, Andrea and Lauro, with whom I have had countless experiences during these two years. Thanks to you I have learned that studying is not at all about competing but about learning, having fun and finding interest, curiosity and passion in what you study.

Finally, many thanks to all my family and friends. From near and far, you have always been supporting me and encouraging me to pursue my dreams.

Popular Science Summary

Measuring the properties of extremely short bursts of light

Did you know that we can produce light in pulses that last only a few femtoseconds (0.000 000 000 000 001 s)? In many applications it is essential to have a precise characterisation of these light pulses. Since there is no event short enough to measure them, the solution lies in manipulating light for its own measurement.

These extremely short bursts of light are known as ultrashort laser pulses. The field of ultrafast science has benefited greatly from them, for the following reason: in order to observe an event, another event that can be controlled and that happens in an even shorter time is needed. This became a problem when scientists first tried to study the motion of atoms and molecules when a chemical reaction occurs, or the electron dynamics in the event of photoionisation (a photon strips an electron from an atom after collision). Fortunately, ultrashort laser pulses can be used as "flashes of light" that last a millionth of a billionth of a second, which has opened the door to the study of ultrafast processes. However, this is not their only application. When a small amount of energy is put into such a short time then the generated power (energy/time) can reach enormous values, as high as 1 PW (1 000 000 000 000 000 W). This is several orders of magnitude greater than for example the power produced in a nuclear power plant. As a consequence, shining these pulses onto matter leads to different effects such as the nonlinear response of the medium, the generation of a plasma, etc. These processes can be used, for example, to cut materials with micrometer precision (0.000 001 m) or to accelerate particles to almost the speed of light (300 000 000 m/s) in a space no larger than a table.

Linked to the generation of ultrashort laser pulses is the need for their characterisation. Just as in a camera it is important to control the exposure time, it is essential to know precisely the duration of these pulses. Another property that is important to control is the polarisation of light. Light is an electromagnetic wave and the polarisation describes the direction it oscillates. In a similar way to how the waves of the sea shape the medium through which they propagate, the oscillations of light induce the movement of electrons, atoms and molecules.

Electronic instruments cannot be used to measure the properties of ultrashort laser pulses, simply because they are not fast enough. Fortunately, there are many ways to manipulate light using optical elements such as lenses, prisms, crystals, among other things that do not require electronics. The key to measure pulses is to manipulate light itself for their own measurement, which has opened the door to a series of methods to measure their duration. In this project we have used one of these methods, called the dispersion scan (d-scan), to measure not only the duration but also the polarisation of ultrashort laser pulses.

Contents

Chapter 1

Introduction

The development of chirped pulse amplification [1], passive mode locking [2] and the availability of high-gain media over a wide frequency range such as titanium-sapphire [3] has standardised the use of femtosecond lasers. This has opened the doors to a great number of applications in the field of ultrafast science: from the studies of chemical reactions [4] and the motion of electrons and molecules [5] to the acceleration of particles [6]. In addition, femtosecond lasers have also proven to be a very useful tool outside of fundamental science, with multiple applications such as refractive surgery [7] and micromachining of materials [8].

In many of these applications precise knowledge of the pulse duration and the shape of the envelope is needed. Therefore, the characterisation of ultrashort laser pulses has become as important as the process of generation. In recent decades, a large number of techniques have been developed for this purpose. The most well-known, listed in chronological order, are the autocorrelation method [9], frequency-resolved optical-gating (FROG) [10] and spectral interferometry for direct electric-field reconstruction (SPIDER) [11]. More recently, a technique called the dispersion scan (d-scan) has been developed [12].

This thesis focuses on the characterisation of ultrashort laser pulses with the d-scan technique.

1.1 Objective

The present project aims to include the measurement of a time-dependent polarisation state in the dispersion scan. A conventional d-scan can retrieve the spectral phase of ultrashort laser pulses and thus together with a separately measured spectrum obtain the pulse profile in the time domain. The problem of reconstructing the polarisation state can be reduced to reconstructing two linearly polarised pulses corresponding to two different projections of the electric field and measuring their relative phase. In principle, one could do this by measuring a total of three different linearly polarised projections of the electric field since the third one contains information about the relative phase difference between the other two. Although

this has already been proven to be possible with FROG [13, 14], it has not been demonstrated with the d-scan yet.

Three challenges are posed to achieve this goal: (i) to design an experimental method capable of generating a time-dependent polarisation state in an accurate and reproducible way, (ii) to adapt the conventional d-scan setup to measure linear projections of the electric field, and finally (iii) to be able to accurately simulate both the time-dependent polarisation and the d-scan measurements to evaluate the performance of the method.

1.2 Motivation

An important property of light, which describes its vectorial nature, is polarisation. In general, the way light interacts with matter is affected by its polarisation, which makes it a great tool for studying the properties of matter.

The motion of atoms and molecules occurs on very short time scales. Because of this, it has only been possible to study thanks to the development of ultrafast laser systems. Therefore, the idea of tailoring the polarisation of ultrashort laser pulses can allow the study of the motion and properties of atoms and molecules that are sensitive to the polarisation of light.

Ultrashort laser pulses with a spatially or temporally varying polarisation are known as vector pulses [15, 16]. In recent years, many methods have been devised to generate pulses with a space-dependent polarisation state, such as radially and azimuthally polarised beams. This has been done by means of optically active wave plates (q-wave plate) [17], azimuth-dependent half-wave plates (s-wave plate) [16] among other methods. One method to modulate the ellipticity of the polarisation state as a function of time, i.e. to generate time-dependent polarisation states, consists in transmitting the pulses through a combination of birefringent plates. The polarisation state originating from this falls into the group of time-dependent polarisation states known as polarisation gates (PGs) [18, 19]. This type of pulse is often used in high-order harmonic generation (HHG) to generate isolated attosecond pulses [20, 21]. The reason for this lies in the strong dependence of the emission efficiency of high-order harmonics on the ellipticity of the fundamental driving field [18, 22, 23]. During the period of time, when the electric field is linear, that is, an ellipticity angle of $0°$, the emission efficiency of higher order harmonics is much higher than when the polarisation is elliptical. Studies have shown that for ellipticities greater than 13% the emission efficiency of plateau harmonics (orders from $q = 19$ to $q = 27$) reduces to 50% in relation to the same harmonics generated with 0% ellipticity [18]. Because the emission of XUV radiation can be confined to an interval of time shorter than the pulse duration, this technique receives the name of polarisation gating. Other examples of application of polarisation in the ultrafast time scale are studies of molecular chirality [24, 25], plasmons [26] and magnetic materials [27].

Linked to the generation of ultrashort laser pulses with a time-dependent polar-

isation state is the need for their characterisation. One of the oldest methods to measure the time evolution of a polarisation state was time resolved ellipsometry (TRE) [28]. This technique is very laborious, it requires the rotation of wave plates and polarisers to select different projections of the electric field and for each of them to measure the cross-correlation with a reference pulse through a nonlinear process while scanning the time of delay between the two. A simpler approach is followed in the dual-channel spectral interferometry method [29], known as POLLIWOG, where two orthogonal components of the pulse to be measured are characterised relative to a well-known reference pulse using spectral interferometry [30]. A different approach is to use a common method for characterising scalar pulses, i.e. pulses with linear polarisation constant in time, and measure the amplitude and phase of the pulse for three different projections. Using SHG-FROG it has been shown that this is sufficient to reconstruct both the polarisation and the temporal characteristics of the pulse [13]. Very recently, this approach has been applied to reconstruct the pulse from a single measurement [14], where instead of measuring three projections, the angle of the polariser is rotated in parallel to the characterisation of the pulse. All of these methods require a reference pulse. For this reason, it would be very good to show that the vector reconstruction of the pulse can also be achieved using an in-line and more stable method such as the d-scan.

Figure 1.1 aims at visualising a pulse with a time-dependent polarisation state by showing the result of a simulation:
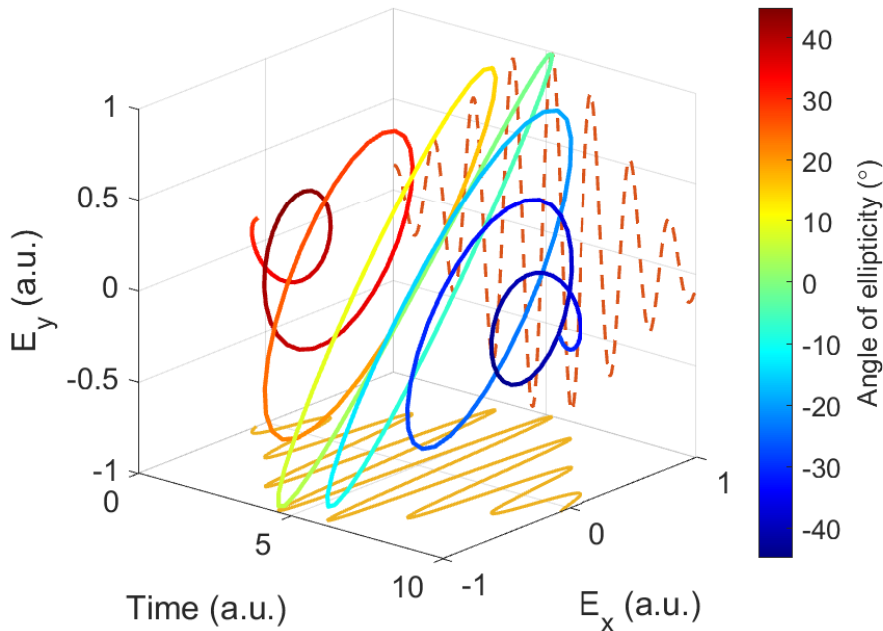

Figure 1.1: Simulation of a pulse with time-dependent polarisation state. The colored line represents the evolution of the electric field endpoint as a function of time, where the color indicates the ellipticity of the polarisation state. The lines on the bottom and in the background represent the horizontal and vertical projections of the electric field, respectively.

1.3 Thesis outline

With the intention of giving a theoretical framework for the project, Chapter 2 covers a summary of polarisation, nonlinear and ultrafast optics, with special emphasise on the concepts relevant to this work. Next, Chapter 3 covers a detailed explanation of the experimental methods as well as how to model and simulate the experiments conducted in the laboratory. In Chapter 4, the most important results of the work are collected and a discussion of them is presented. The thesis concludes with Chapter 5, where a general assessment of the work is made as well as a reflection on possible future steps.

Chapter 2

Theory

This section aims to provide a description of some fundamentals of optics relevant to this work that will help understand the concept behind the d-scan technique, how to simulate the experiments conducted in the scope of this thesis and the interpretation of the measurements. The theoretical framework is divided into three parts: polarisation, nonlinear and ultrafast optics. Two textbooks have frequently been used as sources of inspiration for the theoretical derivations [31, 32].

Polarisation optics covers an introduction to the electromagnetic theory of light, with the main goal of describing the three most common methods that can be used to describe and represent the polarisation state of light. Nonlinear optics is introduced with a brief description of the interaction between light and matter based on the atomic oscillator model. Special attention is paid to the explanation of phase-matching and second harmonic generation (SHG), as the latter process is the means by which the d-scan setup used in the laboratory achieves sensitivity to spectral phase. The last section is dedicated to ultrafast optics. The following topics are discussed there: a theoretical model to describe optical pulses, the role of dispersion in transforming pulse shape upon propagation and a summary of very relevant techniques for the characterisation of ultrashort laser pulses, including d-scan.

2.1 Polarisation Optics

Light is an electromagnetic wave. The wavefront and amplitude of this wave may vary depending on the source of electromagnetic field and the observation distance from it. For instance, a spherical wave originates from a point source and the amplitude decays with the radial distance due to conservation of energy. Another common example are plane waves, which have a planar wavefront and maintain constant amplitude upon propagation.

As an electromagnetic wave, light satisfies Maxwell's equations. In the simple case of a plane wave, this leads to waves with mutually perpendicular electric and magnetic fields, which lie in a plane that is normal to the direction of propagation. This type

of wave is called transverse electromagnetic (TEM) and it is a good approximation for the Gaussian beam. Due to the orthogonality condition it is sufficient to know the electric field (or the magnetic field) in order to have a complete description of the total electromagnetic field. An expression for an electromagnetic plane wave of frequency ν, angular frequency $\omega = 2\pi\nu$ and wavenumber $k = \omega/c$ can be written as follows:

$$\mathbf{U}(\mathbf{r},t) = \mathbf{E}(\mathbf{r}) \exp\left[i\left(\omega t - kz\right)\right] = \left(E_x\hat{\mathbf{x}} + E_y\hat{\mathbf{y}}\right) \exp\left[i\left(\omega t - kz\right)\right] \tag{2.1}$$

where $\mathbf{E}$ is the electric field complex amplitude. E_x and E_y represent the components of the electric field complex amplitude in two orthogonal directions, respectively. One can also rewrite this expression using the magnitude of these complex values, the relative phase difference between each other and a global phase term:

$$\mathbf{U}(\mathbf{r},t) = e^{i\phi}\left(|E_x|\hat{\mathbf{x}} + e^{i\varphi}|E_y|\hat{\mathbf{y}}\right) \exp\left[i\left(\omega t - kz\right)\right] \tag{2.2}$$

Conventionally the polarisation of light refers to the direction of the oscillations of the electric field. One often refers to the real part of the complex electric field $\mathbf{U}$ as the electric field $\mathcal{E}$. Using Equation 2.1 one can arrive to a simplified equation for the electric field:

$$\mathcal{E}(\mathbf{r},t) = \Re\{(E_x\hat{\mathbf{x}} + E_y\hat{\mathbf{y}}) \exp\left[i\left(\omega t - kz\right)\right]\} = \mathcal{E}_x\hat{\mathbf{x}} + \mathcal{E}_y\hat{\mathbf{y}} \tag{2.3}$$

where the two components can be expressed as:

$$\mathcal{E}_x = a_x \cos\left(\omega t - kz + \varphi_x\right) \tag{2.4}$$
$$\mathcal{E}_y = a_y \cos\left(\omega t - kz + \varphi_y\right) \tag{2.5}$$

Three of the most common methods to describe polarisation are introduced below.

2.1.1 Jones Calculus

Polarisation of light can be described using Jones calculus. In this formalism, light is represented by a vector consisting of two components. This is called Jones vector ($\mathbf{J}$) and the two components correspond to the magnitude of the electric field complex amplitude in two orthogonal directions, $|E_x|$ and $|E_y|$, where one of them is multiplied by the relative phase difference $e^{j\varphi}$.

$$\mathbf{J} = \begin{bmatrix} |E_x| \\ |E_y|e^{i\varphi} \end{bmatrix} \tag{2.6}$$

A pure polarisation state is completely determined knowing two orthogonal amplitudes and their relative phase difference. Any pure state of polarisation can be said to be elliptical and expressed as a Jones vector as shown in Equation 2.6. Two special cases of elliptical polarisation are linearly and circularly polarised light. Below are some examples of common polarisation states described using Jones formalism:

Table 2.1: Jones vectors for different states of polarisation.

State of polarisation	Jones vector ($\mathbf{J}$)
Horizontal Linear Polarisation	$\begin{bmatrix} 1 \\ 0 \end{bmatrix}$
Vertical Linear Polarisation	$\begin{bmatrix} 0 \\ 1 \end{bmatrix}$
Right Circular Polarisation (RCP)	$\frac{1}{\sqrt{2}} \begin{bmatrix} 1 \\ i \end{bmatrix}$
Left Circular Polarisation (LCP)	$\frac{1}{\sqrt{2}} \begin{bmatrix} 1 \\ -i \end{bmatrix}$

Commonly, matrices are used to calculate the evolution of light through an optical system. An optical element can be described by a Jones matrix. This is shown in Equation 2.7, where $\mathbf{J}''$, $\mathbf{J}'$ represent the Jones vector of light before and after the optical element and $\mathbf{M_J}$ the Jones matrix of the latter.

$$\mathbf{J}' = \mathbf{M_J} \cdot \mathbf{J}'' \tag{2.7}$$

In the following, as an example, it is detailed how to write the Jones matrix of the optical elements used during the experiments. When light goes through a linear polariser it gets linearly polarised along the direction defined by the polariser axis. Therefore, vertical and horizontal polarisers will select, respectively, the first and second components of the incoming Jones vector and cancel the other one.

Table 2.2: Jones matrices for horizontal and vertical polarisers.

Polariser	Jones matrix ($\mathbf{M_J}$)
Horizontal polariser	$\begin{bmatrix} 1 & 0 \\ 0 & 0 \end{bmatrix}$
Vertical polariser	$\begin{bmatrix} 0 & 0 \\ 0 & 1 \end{bmatrix}$

Wave plates, also known as wave retarders, are made from birefringent materials. A medium is said to be birefringent when optical properties like the refractive index n depend on the direction of polarisation of light. A 3-dimensional representation of a birefringent crystal is given by the index ellipsoid, shown in Figure 2.1:
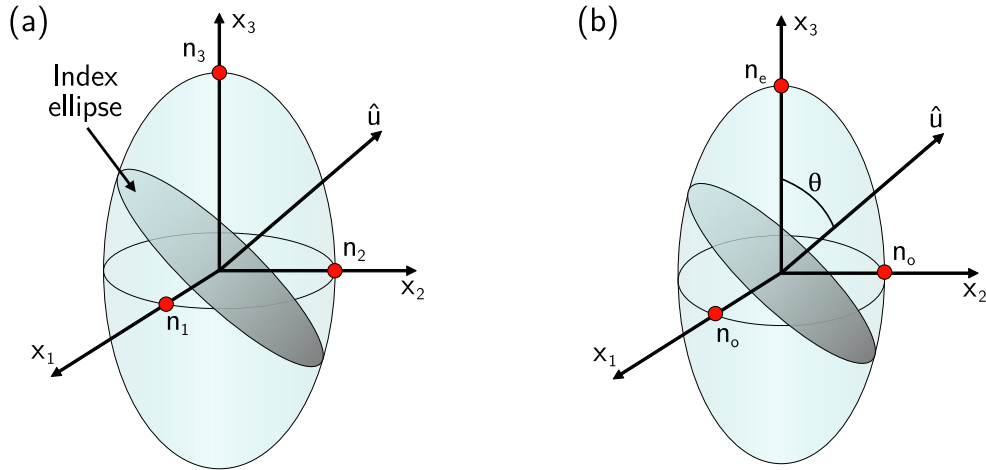
Figure 2.1: The index ellipsoid. The index ellipsoid is a geometric representation of a tensor whose principal axes and eigenvalues are denoted respectively by the coordinates (x_1, x_2, x_3) and the refractive indexes (n_1, n_2, n_3). (a) Index ellipsoid of a biaxial crystal. (b) Index ellipsoid of a uniaxial crystal.

The semi-axes lengths of the index ellipsoid correspond to the value of the refractive index in three orthogonal directions of the crystal. Depending on the relation between these values, three types of birefringent crystal can be defined: isotropic when $n_1 = n_2 = n_3$, uniaxial when $n_1 = n_2 = n_o$ and $n_3 = n_e$ and biaxial, when $n_1 \neq n_2 \neq n_3$. Uniaxial crystals are also subdivided into positive or negative crystals depending on whether $n_e > n_o$ or vice versa.

For any plane wave propagating along a direction defined by a vector $\hat{\mathbf{u}}$ the intersection between a plane perpendicular to this vector and the index ellipsoid forms an ellipse, known as the index ellipse. The lengths of the semi-axes of this ellipse represent the refractive indexes associated with the two orthogonal polarisations of light travelling on the direction defined by $\hat{\mathbf{u}}$. A special case is when the polarisation ellipse becomes a circle. This happens when light propagates along a specific direction within the birefringent crystal, which is known as the optic axis. In uniaxial crystals, this direction is aligned with the extraordinary axis, that is, the direction for which $n = n_e$.

The semi-axes lengths of the polarisation ellipse in a uniaxial crystal correspond to the ordinary n_o and extraordinary $n(\theta)$ refractive indexes, where θ is the angle between $\hat{\mathbf{u}}$ and the extraordinary axis. A simple formula, given in Equation 2.8 can be used to calculate $n(\theta)$:

$$\frac{1}{n^2(\theta)} = \frac{\cos^2(\theta)}{n_o^2} + \frac{\sin^2(\theta)}{n_e^2} \tag{2.8}$$

Uniaxial crystals are typically the material from which wave plates are made. The optic axis is parallel to the polished surface of the crystal so that different polarisations will sense a different refractive index. The difference in refractive index between two orthogonal polarisations causes a phase delay between them. This relative phase shift is proportional to the propagation distance inside the crystal (d).

Considering the extraordinary and ordinary axes, which are known as the principal axes of the wave plate, the exact phase delay can be calculated as shown in Equation 2.9:

$$\Delta\varphi = \Delta k \cdot d = \frac{2\pi}{\lambda_0}\left(n_{\mathrm{e}} - n_{\mathrm{o}}\right)d \tag{2.9}$$

In a frame of reference where horizontal and vertical polarisations are aligned with the principal axes of the wave plate, the Jones matrix of this element becomes diagonal and can be expressed as:

$$\mathbf{M_J} = \begin{bmatrix} 1 & 0 \\ 0 & e^{i\Delta\varphi} \end{bmatrix} \tag{2.10}$$

The most commonly used wave plates are quarter- and half- wave plates that add a phase shift of $\pi/2$ and π, respectively, between the fast and slow axes. They are frequently used to change the state of polarisation of light. For example, a quarter-wave plate can convert circular polarisation into linear while a half-wave plate can be used to rotate a linearly polarised state to any other angle.

Table 2.3: Jones matrices for quarter- and half-wave plates.

Waveplate	Jones matrix ($\mathbf{M_J}$)
Quarter-wave plate	$\begin{bmatrix} 1 & 0 \\ 0 & i \end{bmatrix}$
Half-wave plate	$\begin{bmatrix} 1 & 0 \\ 0 & -1 \end{bmatrix}$

The elements of the Jones matrix are dependent on the coordinate system of choice. Nevertheless, knowledge of the diagonal form of the matrix is sufficient if rotation matrices are used to transform this matrix into another coordinate system, whose directions make an angle θ in respect to the coordinate system where the matrix is diagonal. This transformation is written as a matrix product in Equation 2.11:

$$\mathbf{M'_J} = \mathbf{R}(-\theta) \times \mathbf{M_J} \times \mathbf{R}(\theta) \tag{2.11}$$

Where $\mathbf{R}(\theta)$ represents the rotation matrix, calculated as follows:

$$\mathbf{R}(\theta) = \begin{bmatrix} \cos(\theta) & \sin(\theta) \\ -\sin(\theta) & \cos(\theta) \end{bmatrix} \tag{2.12}$$

This is especially useful for wave plates, as they must not be aligned with the input polarisation for them to have any effect on the polarisation state. Very often a relative orientation of 45° is used, since in this case the amplitude of the electric field is divided equally between the two principal directions of the plate.

2.1.2 Polarisation Ellipse

On a plane perpendicular to the direction of propagation, tracing the evolution over time of the electric field endpoint results in the drawing of an ellipse, which is known as the ellipse of polarisation. A parametric equation of the ellipse can be derived from Equations 2.3, 2.4 and 2.5:

$$\frac{\mathcal{E}_x^2}{a_x^2} + \frac{\mathcal{E}_y^2}{a_y^2} - 2\cos\left(\varphi_y - \varphi_x\right)\frac{\mathcal{E}_x\mathcal{E}_y}{a_x a_y} = \sin^2\left(\varphi_y - \varphi_x\right) \tag{2.13}$$

An example of the polarisation ellipse is shown in Figure 2.2. Here a and b are the lengths of the semi-major and semi-minor axes, respectively. The two angles that define the ellipse are indicated in this figure. ψ is the angle between the x axis and the major axis of the ellipse, that is, it measures the relative orientation of the ellipse with respect to a fixed frame of reference defined by the $\hat{\mathbf{x}}$ and $\hat{\mathbf{y}}$ directions. χ is the angle of ellipticity, which can be calculated as the arc-tangent of the ratio between b and a. When $\chi = 0°$ the ellipse degenerates into a line. Regarding the state of polarisation, this indicates that the electric field vibrates along a line, which means that it is linearly polarised (LP). On the other hand, when $\chi = 45°$, the ellipse degenerates into a circle. This indicates that light has a circular state of polarisation (CP). The angle of ellipticity can take negative values to represent the opposite direction of rotation. For example, the electric field is said to be right circularly polarised (RCP) when $\chi = +45°$ while left circularly polarised (LCP) when $\chi = -45°$.
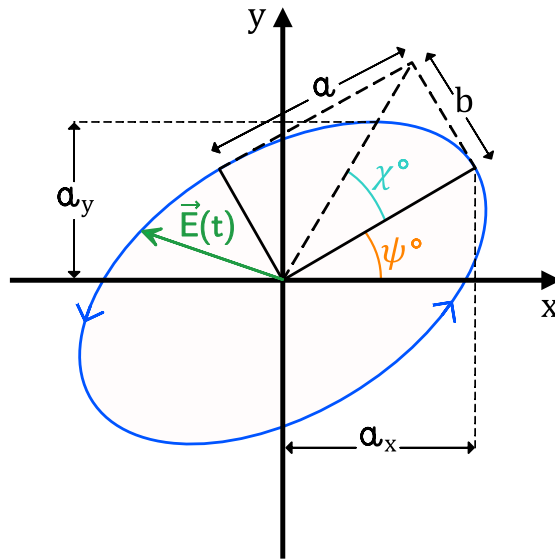

Figure 2.2: The polarisation ellipse. During an optical cycle the end point of the electric field traces an ellipse, known as polarisation ellipse.

To draw the polarization ellipse it is enough to know the angles χ and ψ. From these two variables it is possible to determine the phase difference $(\varphi = \varphi_y - \varphi_x)$ and the amplitude ratio $(R = a_y/a_x)$ between two orthogonal directions, x and y, for example. The relationship between these variables is shown in Equations 2.14 and 2.15:

$$\tan 2\psi = \frac{2R}{1 - R^2} \cos \varphi \tag{2.14}$$

$$\sin 2\chi = \frac{2R}{1 + R^2} \sin \varphi \tag{2.15}$$

Hence, from the polarisation ellipse one can reconstruct the total electric field and vice versa.

2.1.3   Poincaré Sphere

The orientation of the polarisation ellipse can vary from $\psi = 0°$ to $\psi = 180°$. Similarly, its angle of ellipticity can vary from $\chi = -45°$ to $\chi = 45°$. As represented in Figure 2.3a, using a spherical coordinate system, where the angles 2ψ and 2χ act as azimuthal and polar angles, respectively, one can construct a sphere with unit radius that encodes information about polarisation since every point on its surface will represent a pure state of polarisation. Additionally, the radius of the sphere represents the intensity of light. This 3-dimensional representation of the polarisation is known as the Poincaré sphere, which is depicted in Figure 2.3.
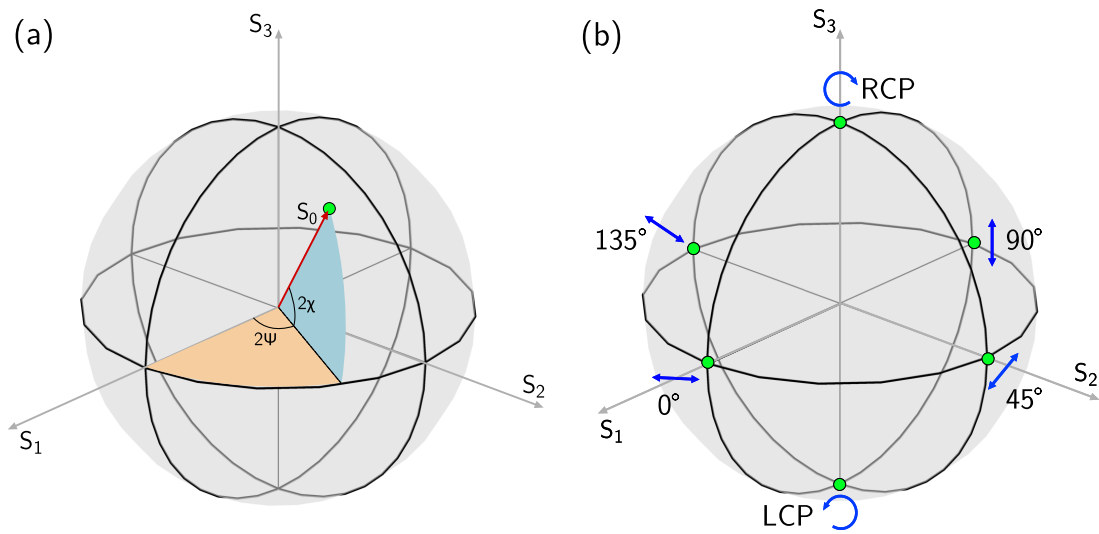

Figure 2.3: The Poincaré sphere. Any polarisation state can be represented on the surface of the Poincaré sphere using the angles of orientation (ψ) and ellipticity (χ) of the polarisation ellipse as spherical coordinates. (a) Coordinates. (b) Common polarisation states.

Equations 2.17, 2.18 and 2.19 are the Cartesian coordinates (x, y and z) of the points on the Poincaré sphere. These are also the definitions of the Stokes parameters (S_1, S_2 and S_3) where S_0 is the intensity of light and represents the radius of the sphere. As seen in Figure 2.3b, points along the equator correspond to linear states of polarisation. Each hemisphere correspond to an opposite direction of rotation (different

handedness) and the vertices of the sphere correspond to circularly polarised states, right circularly polarised (RCP) and left circularly polarised (LCP) respectively.

$$S_0 = I_x + I_y \tag{2.16}$$
$$S_1 = x = S_0 \cos 2\chi \cos 2\psi \tag{2.17}$$
$$S_2 = y = S_0 \cos 2\chi \sin 2\psi \tag{2.18}$$
$$S_3 = z = S_0 \sin 2\chi \tag{2.19}$$

Although the Poincaré sphere representation of a polarisation state requires more calculations than the previous methods and might seem not very intuitive at first, it has the advantage of being able to associate any state of polarisation to a point on the same surface, which makes it a very good visualisation method.

2.2   Nonlinear Optics

When an electric field interacts with an atom, it induces a dipole moment by dinamically displacing the electron cloud from the nucleus. Similarly, an EM wave induces an oscillating dipole moment ($\mathbf{p}$) proportional to the charge of the atom (q) and the charge displacement (Δx), which in turn acts as source of a second EM wave with the same frequency as the first one (see Figure 2.4).
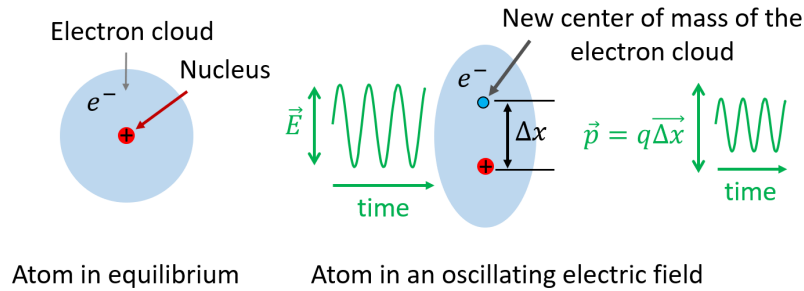

Figure 2.4: Induced polarisation in a single atom.

If a group of atoms is considered, the contribution of every atomic oscillator induces a total dipole moment, often described as polarisation density ($\mathbf{P} = N\mathbf{p}$), which can be calculated as the sum of the individual dipoles. This magnitude is frequently expressed in terms of the vacuum permitivity (ε_0), the susceptibility of the medium (χ) and the electric field of the incoming wave ($\mathbf{E}$), as shown in Equation 2.20:

$$\mathbf{P} = N\mathbf{p} = \varepsilon_0 \chi \mathbf{E} \tag{2.20}$$

An sketch of an electric field interacting with a group of atoms is depicted in Figure 2.5.
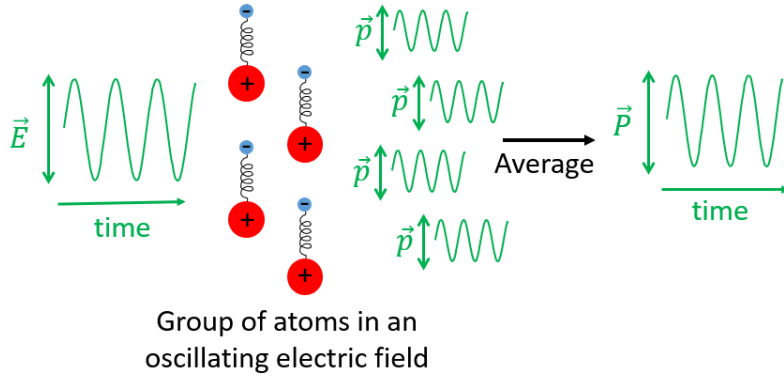
Figure 2.5: Induced polarisation in a group of atoms.

Equation 2.20 is only valid in linear dielectric media, which are characterised by having a linear relation between the polarisation and the electric field. Nonlinear dielectric media, on the other hand, are characterised by having a nonlinear relation between them. To extend this equation to nonlinear media one can express the polarisation density using a Taylor series expansion, as shown in Equation 2.21:

$$\mathbf{P} = \mathbf{P}^{(1)} + \mathbf{P}^{(2)} + \mathbf{P}^{(3)} + \cdots = \varepsilon_0 \left(\chi^{(1)}\mathbf{E} + \chi^{(2)}\mathbf{E}^2 + \chi^{(3)}\mathbf{E}^3 + ... \right) \tag{2.21}$$

In many situations, the linear approximation ($\mathbf{P}^{(1)}$) is sufficiently precise and one can neglect higher-order terms. However, one needs to start considering them when the magnitude of the electric field is high enough that the medium has a significant nonlinear response. Each high-order term of the polarisation is associated to different frequency components. For example, expanding the second and third order terms gives:

$$\mathbf{P}^{(2)} = \varepsilon_0\chi^{(2)}\mathbf{E}_0^2 \left[\cos(2\omega t + 2kz) + 1\right] \tag{2.22}$$

$$\mathbf{P}^{(3)} = \varepsilon_0\chi^{(3)}\mathbf{E}_0^3 \left[\cos(3\omega t + 3kz) + \cos(\omega t + kz)\right] \tag{2.23}$$

Here one can see that by sending light into a nonlinear medium, it is possible to generate EM waves oscillating at two times (2ω) and three times (3ω) the original frequency. These are known as the second- and third-order harmonics and can be used in multiple applications. Additionally, a DC component follows from the expansion of the second-order nonlinearity. This is the reason why optical pulses can create DC voltages in a process known as optical rectification. Furthermore, the expansion of the third-order term leads to an ω oscillation of the polarisation density. This can be interpreted as a nonlinear dependence of the refractive index of the nonlinear medium with the intensity of light, a phenomenon known as the Optical Kerr effect.

2.2.1 Three-Wave Mixing

It is of special interest to study what happens when an optical field with two frequency components $\mathbf{E}(\omega_1, \omega_2)$ is sent into a nonlinear medium:

$$\mathbf{E}(\omega_1, \omega_2) = \mathbf{E}(\omega_1) \exp\left[i(\omega_1 t - k_1 z)\right] + \mathbf{E}(\omega_2) \exp\left[i(\omega_2 t - k_2 z)\right] \tag{2.24}$$

The induced polarisation density oscillates with different frequency components: 0, $2\omega_1$, $2\omega_2$, $\omega_1 + \omega_2$ and $\omega_1 - \omega_2$. As a result of mixing the two waves, waves with all these different frequencies can be generated but the conversion efficiency is generally different. The reason for this is that a constructive phase relation between the generated waves needs to be maintained over time and space.

For simplicity, this process can be regarded as the interaction between three waves with frequencies ω_1, ω_2 and ω_3. Energy can be transferred between them but according to photon energy conservation, the total energy must be conserved. This is referred to as the frequency-matching condition, shown in Equation 2.25:

$$\omega_1 + \omega_2 = \omega_3 \tag{2.25}$$

One also needs to consider that the third wave can be generated in any point inside the nonlinear medium. Therefore, in order to generate a strong nonlinear signal there needs to be constructive interference between the generated waves along the direction of propagation. As represented in Figure 2.6, a sum of phasors can be destructive or constructive depending on the phase relation:
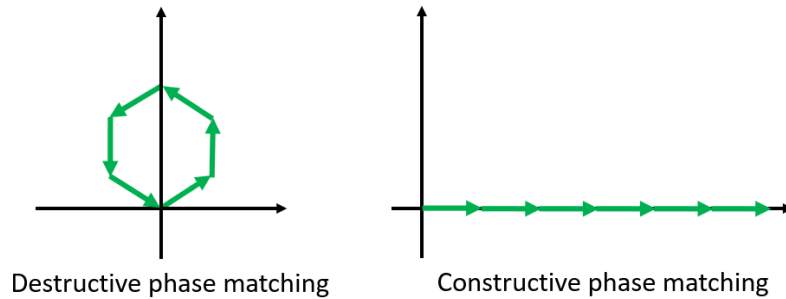

Destructive phase matching   Constructive phase matching

Figure 2.6: Schematic of destructive and constructive interference with phasors.

A mathematical expression of the phase-matching condition is shown in Equation 2.26 with the sum of the wavevectors:

$$\mathbf{k_1} + \mathbf{k_2} = \mathbf{k_3} \tag{2.26}$$

In collinear wave mixing this expression can be rewritten as:

$$n_1 k_1 + n_2 k_2 = n_3 k_3 \tag{2.27}$$

Due to the presence of chromatic dispersion $(n(\lambda))$ in the nonlinear medium, different wavelengths will experience a different refractive index and this needs to be accounted in order to achieve phase-matching.

2.2.2 Second Harmonic Generation

A degenerate case of three-wave mixing is the process of second harmonic generation (SHG), where $\omega_1 = \omega_2 = \omega$ and $\omega_3 = 2\omega$. The phase-matching condition in the collinear case can then be simplified to:

$$n(\omega) = n(2\omega) \tag{2.28}$$

Because of chromatic dispersion this condition cannot be satisfied in many optically transparent crystals. A very common solution to compensate for dispersion is to use birefringent media. This adds an additional degree of freedom since the refractive index also depends on the light polarisation. There are two types of wave mixing depending on whether the polarisation of ω_1 and ω_2 is the same (Type-I wave mixing) or not (Type-II wave mixing). In uniaxial crystals, there are again two possibilities: either the incident beam is ordinary polarised and the second harmonic is extraordinary polarised or vice versa. These two processes are known as ooe and eeo SHG, respectively. Phase-matching can only be achieved in one of them and which one will depend on whether the material is a positive or negative uniaxial crystal. The phase-matching condition is written in Equations 2.29 and 2.30 for ooe and eeo SHG, respectively:

$$n_{\mathrm{o}}(\omega) = n_{\mathrm{e}}(\theta, 2\omega) \tag{2.29}$$
$$n_{\mathrm{e}}(\theta, \omega) = n_{\mathrm{o}}(2\omega) \tag{2.30}$$

Figure 2.7 aims at visualising birefringent phase-matching. First, Figure 2.7a shows the dependence of the refractive index on frequency for both the ordinary and the extraordinary index. It is shown that the extraordinary index at ω is equal to the ordinary index at 2ω, satisfying the phase-matching condition for eeo Type-I SHG. Next to it, Figure 2.7b shows a different picture where the refractive index dependence is plotted as a function of the angle θ between the direction of propagation and the optic axis of the crystal. For the direction marked with a black line, the ellipse described by $n_{\mathrm{e}}(\theta,\omega)$ intersects the circle described by $n_{\mathrm{o}}(2\omega)$. This is the direction at which the eeo SHG phase-matching condition is met.
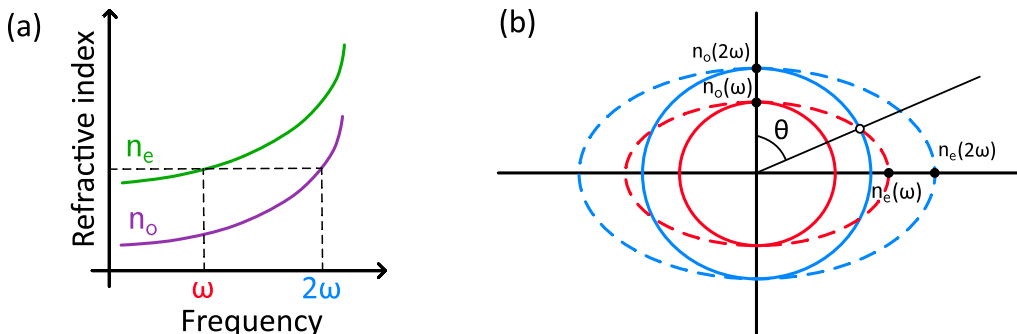

Figure 2.7: Birefringent phase-matching. (a) Matching the index of the extraordinary wave at ω with that of the ordinary wave at 2ω. (b) Ordinary and extraordinary refractive indexes at ω and 2ω as a function of the angle θ between optic axis and the direction of propagation. Adaptation from [31].

2.3 Ultrafast Optics

The measurement of ultrashort laser pulses is of high relevance to this work. For preparing such a setup and being able to extract useful properties from the measurements, one first needs to understand what an optical pulse is and what phenomena affects its propagation, especially through air, but also through different materials. To provide a helpful theoretical background, here there is a brief introduction to ultrafast optics, divided into three parts: fundamentals, propagation and characterisation of optical pulses.

2.3.1 Fundamentals of Optical Pulses

A wave is said to be monochromatic when it oscillates sinusoidally over time with a constant frequency. The sum of two monochromatic waves is represented in Equation 2.31, where $U(t)$ represents the complex wave function:

$$U(t) = \sqrt{I_1}\exp\left(i\omega_1 t\right) + \sqrt{I_2}\exp\left(i\omega_2 t\right) \tag{2.31}$$

The intensity that results from adding two monochromatic waves oscillates at a frequency equal to the difference between the two original frequencies, known as the beating frequency, as shown in Equation 2.32:

$$I(t) = |U(t)|^2 = I_1 + I_2 + 2\sqrt{I_1 I_2}\cos\left[\left(\omega_2 - \omega_1\right)t\right] \tag{2.32}$$

This temporal interference is analogous to the spatial interference between two planes waves travelling at different angles. Keep adding multiple monochromatic waves with a constant frequency spacing gives a beating signal with a shorter temporal width. Thus, the discrete sum of monochromatic light waves results in a train of optical pulses, where each pulse has a duration that decreases with the frequency spacing and the number of added waves (M). Equation 2.33 shows a mathematical expression for the sum of M waves with a constant frequency spacing ω_F and central frequency ω_0:

$$U(t) = \sqrt{I_0}\sum_{q=-L}^{L}\exp\left[i(\omega_0 + q\omega_F)t\right] \tag{2.33}$$

where $M = 2L + 1$. This summation can be solved analytically and Equation 2.34 shows the solution:

$$I(t) = |U(t)|^2 = I_0\frac{\sin^2\left(M\pi t/T_F\right)}{\sin^2\left(\pi t/T_F\right)} \tag{2.34}$$

where is $T_F = 2\pi/\omega_F$.

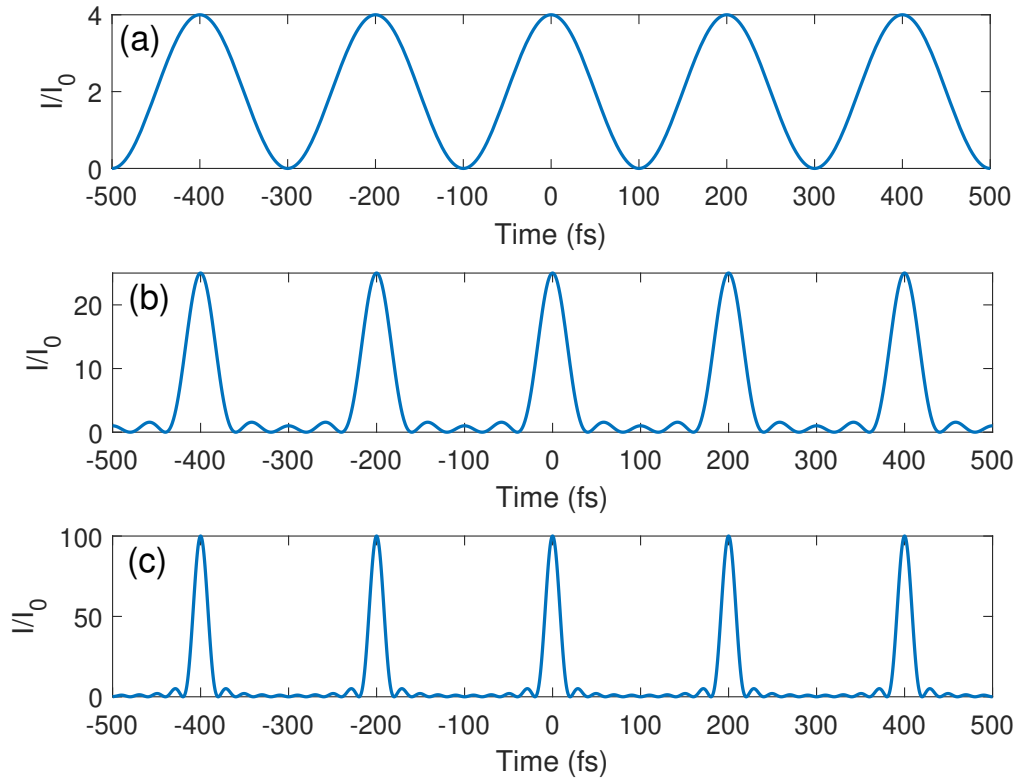The interference of multiple waves can be easily calculated and Figure 2.8 shows three different examples of this:

Figure 2.8: Intensity resulting from the superposition of monochromatic waves. (a) Sum of 2 waves. (b) Sum of 5 waves. (c) Sum of 10 waves.

Here a total of 10 waves are simulated. The first one has a frequency of 375 THz (corresponding to a wavelength of 800 nm) while the other waves have a frequency that is 5 THz (a shift of 11 nm at 800 nm) shifted with respect to the previous one. Clearly, the width of the pulses decreases significantly as the number of interfering waves is increased. In other words, the more frequency components are added to the mix the shorter the duration of the pulse will be. Although here a coherent superposition of waves has been simulated, i.e. with a constant phase difference between them, in reality, this is rarely the case. For example, longitudinal modes from a laser oscillator usually have a random phase relationship. A number of mode-locking techniques that aim at locking the phases of the longitudinal modes of a laser, i.e. maintain a constant phase relation between them, have been developed for this reason [33].

A very important concept that follows from this derivation is the time-bandwidth relation of optical pulses. A full description of the complex electric field of a pulse can be made in both the temporal and in the frequency domains. Both descriptions are equivalent and the transition from one to the other is done by means of the Fourier transform. Equation 2.35 shows how to calculate the spectral amplitude $|\tilde{U}(\omega)|$ and the spectral phase $\phi(\omega)$ from the Fourier transform of the complex electric field in the time domain $U(t)$ [34].

$$\tilde{U}(\omega) = \left|\tilde{U}(\omega)\right| \exp\left[i\phi(\omega)\right] = \int_{-\infty}^{+\infty} U(t) \exp\left(-i\omega t\right)dt \qquad (2.35)$$

A direct consequence of this is that the minimum achievable temporal width of a pulse is inversely proportional to the spectral width. Additionally, in accordance with the properties of the Fourier transform, these two quantities must satisfy the time-bandwidth reciprocity relation. For Gaussian-shaped pulses, this relation is written in Equation 2.36, where the temporal (Δt) and spectral ($\Delta \nu$) widths are expressed as full-width at half-maximum (FWHM) of the intensity. This relation states that for a given bandwidth there is a minimum pulse duration. The shortest possible pulse is said to be transform-limited.

$$\Delta t \cdot \Delta \nu \geq \frac{4 \ln 2^{1/2}}{2} \approx 0.44 \tag{2.36}$$

Optical pulses can have very short duration, less than picoseconds (10^{-12} s), receiving the name of ultrashort optical pulses. These pulses require light to have a broad spectrum. As a practical example, according to Equation 2.36 the bandwidth needed in order to generate a 5 fs transform-limited pulse is $\Delta \nu \approx 88.1$ THz. In terms of wavelength bandwidth this value corresponds to $\Delta \lambda \approx 188$ nm around a central wavelength of $\lambda_0 \approx 800$ nm.

2.3.2 Propagation of Optical Pulses

A pulse of light is composed of a continuum of monochromatic waves, each of them propagating at the speed of light (c), which is often called phase velocity. The fact that phase velocity depends on frequency is a phenomenon known as dispersion [35]. Typically, an expression that links phase velocity to frequency is known as dispersion relation. Waves propagating in vacuum follow quite a simple dispersion relation, written in Equation 2.37:

$$c = \frac{\omega}{k} \tag{2.37}$$

where ω is the angular frequency and k the wavenumber. Another quantity of interest derived from the dispersion relation is the velocity at which the envelope of a pulse propagates, known as the group velocity (v), which is calculated as the partial derivative $\partial \omega / \partial k$ [31]. Through propagation in vacuum, both the phase and group velocities are the same, meaning that the shape of the pulse does not change upon propagation. However, when the pulse travels through a medium different from vacuum the dispersion relation gets more complicated and the pulse shape generally changes upon propagation.

A very common way to quantify the dispersion of a pulse is to look at its spectral phase content. The spectral phase can be approximated by a polynomial expansion, as shown in Equation 2.38:

$$\phi(\omega) = \sum_n \frac{1}{n!} \phi^{(n)}(\omega_0)(\omega - \omega_0)^n \tag{2.38}$$

where $\phi^{(n)}$ represents the nth derivative of the spectral phase function with respect to

the angular frequency, evaluated at a reference angular frequency ω_0. Each of these terms has an important physical meaning. The zero-order (unit-less), $\phi^{(0)}$, is the phase accumulated at the frequency ω_0 and it measures what is the position of the optical reference relative to the peak of the envelope. The first-order (in [fs]), $\phi^{(1)}$, measures the time the optical reference has propagated from where it was generated, assuming it travelled at the vacuum speed of light. The second order (in $\left[\text{fs}^2\right]$), $\phi^{(2)}$, is known as the group delay dispersion (GDD) and it measures the rate of change of the pulse duration as it propagates. Furthermore, the sign of GDD determines whether the pulse has a positive or negative chirp, that is, whether the frequency increases or decreases with time. Regardless of whether the chirp is positive or negative, its presence leads to an increase in the pulse duration (τ) compared to the transform-limited case (τ_0). An expression relating the two quantities is shown in Equation 2.39 [35]:

$$\tau = \tau_0 \sqrt{1 + \frac{16(\ln 2)^2[\phi^{(2)}(\omega_0)]^2}{\tau_0^4}} \tag{2.39}$$

Higher orders, like $\phi^{(3)}$ which is known as third order dispersion (TOD), give additional information about the change of the pulse shape as it propagates. Figure 2.9 shows different examples of how the spectral phase affects the shape of the pulse in the time domain.
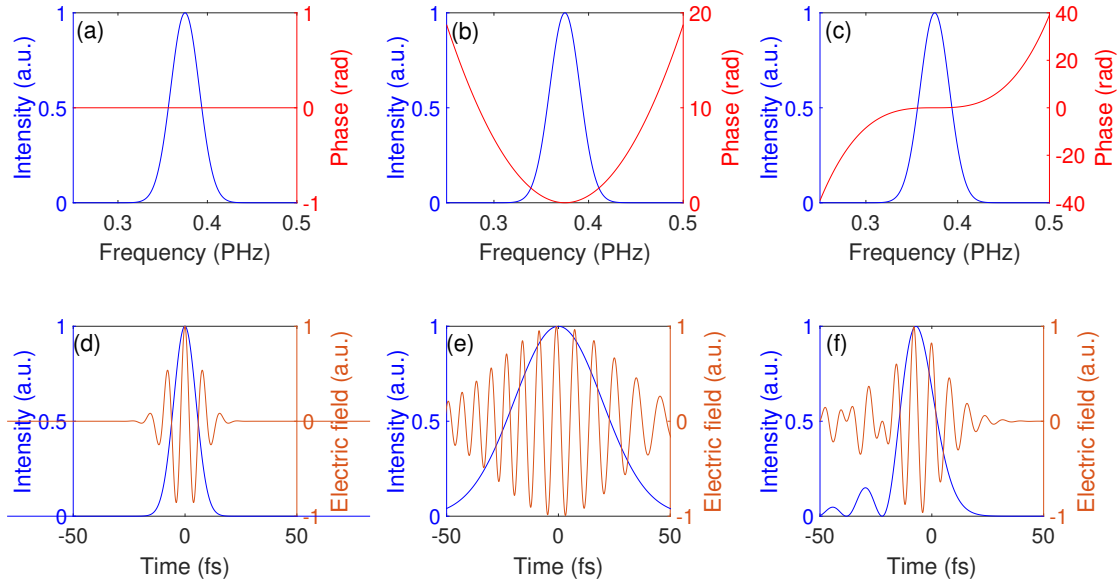

Figure 2.9: Simulations showing the effect of dispersion on the pulse shape. (a)-(c) Envelope and phase of the pulse in the frequency domain. (d)-(f) Envelope and amplitude of the pulse in the time domain.

The origin of dispersion might be attributed to three different phenomena: refraction, diffraction and interference [35]. The first one is associated with the dependence of the refractive index on the frequency of light, mainly due to absorptive resonances. The second one emerges from diffraction and the frequency dependent

deflection that occurs at non-normal incidence between different dielectric media. Finally the third one originates from the interference of waves due to propagation in periodic structures.

The first of these is strongly dependent on which material light is propagating through, which is why it is often referred to as material dispersion. When a pulse of light traverses a medium it acquires a spectral phase that can be written as shown in Equation 2.40:

$$\phi(\omega) = k_0(\omega)n(\omega)d = \frac{\omega}{c_0}n(\omega)d \tag{2.40}$$

The frequency dependence of the refractive index has its origin in the atomic and molecular structure of the material. Atoms and molecules have absorptive resonances at certain frequencies, which causes a nonlinear relation between the refractive index and the frequency, even in spectral regions where the medium presents low absorption. Far away from resonances, this dependence can be easily modelled and it is often described by the Sellmeier equations. For optically transparent materials, these equations provide a good description of the refractive index inside the visible region of the spectrum. The Sellmeier equations for fused silica and BK7 are plotted as a function of frequency and wavelength in Figures 2.10a and 2.10b:
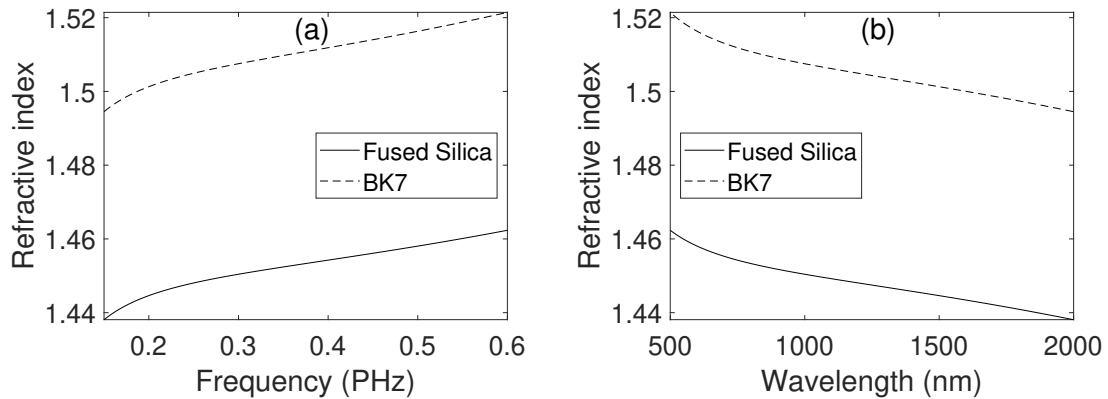

Figure 2.10: Refractive index from Sellmeier equations for fused silica and BK7. (a) As a function of frequency. (b) As a function of wavelength.

By plugging the value of refractive index in Equation 2.40 and numerically derivating, one can calculate the second- and third-order terms of the polynomial expansion of the spectral phase (see Equation 2.38). An example of this calculation for two different materials, fused silica and BK7, is shown in Figure 2.11. Here the second- and third-order terms of the spectral phase, represented respectively by the GVD and TVD, are plotted as a function of both frequency and wavelength. GVD is known as group velocity dispersion and measures the GDD per unit of material insertion. Similarly, the TVD, known as third-order velocity dispersion, measures the TOD per unit of material insertion.
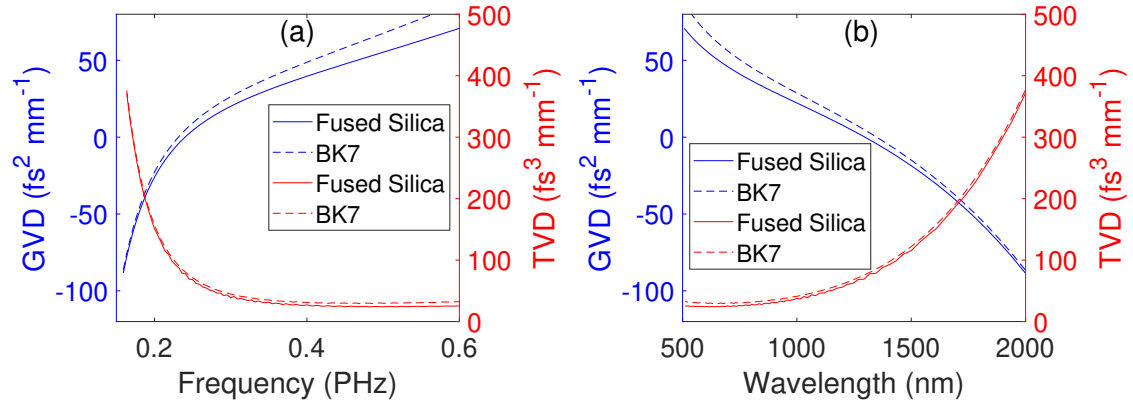
Figure 2.11: Calculated GVD and TVD for fused silica and BK7. (a) As a function of frequency. (b) As a function of wavelength.

2.3.3 Characterisation of Ultrashort Laser Pulses

Many applications of ultrashort laser pulses require their precise characterisation. Sometimes, this means having a complete description of the oscillating electric field, while other times it could be simply measuring the pulse duration. This has led to a very active line of research in recent decades, whose goal has been to develop optical pulse measurement techniques. Generally, when it comes to measuring the duration of an event, other shorter processes are used so as to have an adequate temporal resolution for the first one. This, however, is not possible to do when measuring ultrashort laser pulses, since these are the shortest events that can be generated.

One way to circumvent this issue is using the pulse itself for its own measurement. This is what the autocorrelation technique does. The pulse to be measured is splitted into two replicas, one of which goes into a delay stage. The two pulses are then focused into a crystal, where a nonlinear signal is generated, which is then measured with a photodetector. An sketch of the setup of an autocorrelator using SHG as nonlinear process is depicted in Figure 2.12:
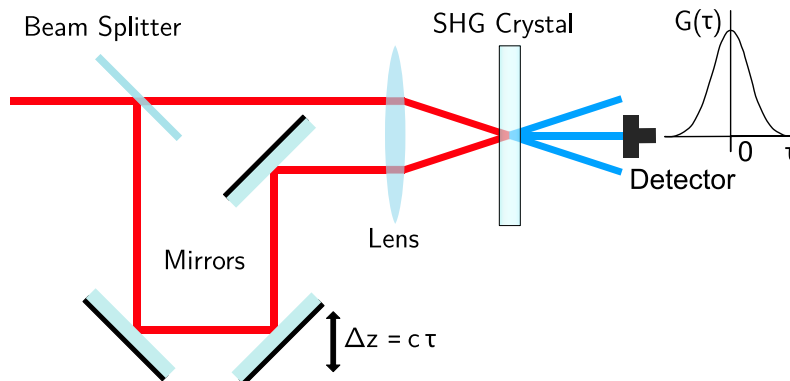

Figure 2.12: Schematic of an autocorrelator.

The intensity of the recorded SHG signal is dependent on the temporal overlap

between the replicas in the crystal. Increasing the overlap results in a stronger signal and vice versa. During a measurement, the signal is recorded while scanning the delay between the two pulses. Plotting the intensity of the SHG signal as a function of the time delay τ yields an autocorrelation signal $G(\tau)$, which is the convolution of the pulse intensity $I(t)$, as shown in Equation 2.41:

$$G(\tau) = \int I(t)I(t-\tau)dt \qquad (2.41)$$

In general, measurement of the pulse autocorrelation is not sufficient to determine the temporal profile of the pulse. As seen in Equation 2.42, from the autocorrelation one can determine the square magnitude of the Fourier transform of the pulse intensity, but knowledge of the spectral phase is needed in order to reconstruct the pulse in the time domain:

$$\mathcal{F}\{G(t)\} = |\mathcal{F}\{I(t)\}|^2 \qquad (2.42)$$

In some cases it is sufficient to make an estimation of the pulse parameters. This can be done, for example, assuming that the pulse is symmetric, i.e. $I(t) = I(-t)$, and therefore has zero phase since the Fourier transform of a symmetric (even) function has no imaginary part. In spite of its limitations, the autocorrelator has proven to be a very simple and useful method to estimate pulse duration. Moreover, the experimental method of correlation between pulses proposed here has served as a basis for many other pulse measurement techniques.

Another well-established technique is frequency-resolved optical gating (FROG) [10]. This method needs a reference pulse, which could be, as in autocorrelation, a replica of the measured one. The two pulses are focused into a nonlinear medium with a controlled delay. Only during the time interval or "time gate" in which the reference pulse passes through the nonlinear medium, the incidence of the measured pulse produces a nonlinear signal that can be detected. Unlike the autocorrelator, FROG additionally resolves the signal with a spectrometer. There are multiple variations of FROG today, especially in terms of how to produce the "time gate". The use of nonlinear processes for this purpose is very common, such as SHG or the optical Kerr effect. Figure 2.13 shows a sketch of a FROG that uses SHG:
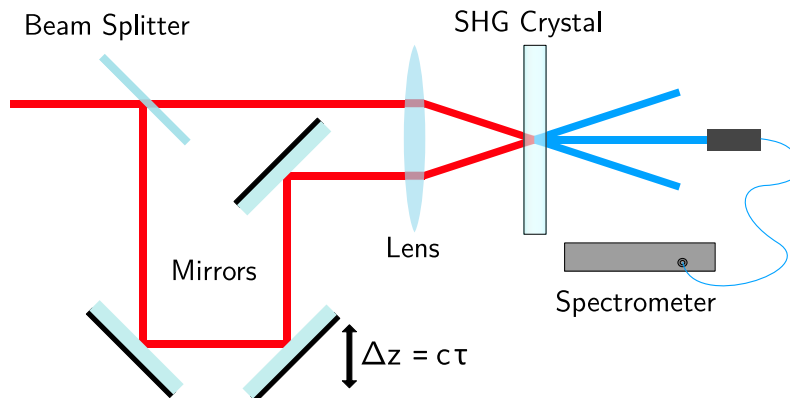

Figure 2.13: Schematic of SHG-FROG.

While it is true that the spectrum recorded for a single time delay still lacks phase sensitivity, the set of measurements obtained after scanning the time delay between the two pulses is sensitive to the spectral phase of the pulse. Plotting the measured spectra with delay time on the vertical axis and frequency on the horizontal results in a spectrogram $S(\nu,\tau)$ known as the FROG trace. An expression for $S(\nu,\tau)$ can be written as follows:

$$S_{\text{FROG}}(\nu, \tau) = |\Phi(\nu,t)|^2 \qquad \Phi(\nu,t) = \int_{-\infty}^{+\infty} g(t,\tau) e^{-i2\pi\nu t} dt \qquad (2.43)$$

Where $g(t,\tau) = U(t)W(t - \tau)$ is the product between the measured optical pulse $U(t)$ and the time-delayed gating function $W(t - \tau)$. Knowledge of $\Phi(\nu,t)$ would be sufficient to estimate $U(t)$. Although the problem of extracting $\Phi(\nu,t)$ from the FROG trace might seem to be unsolvable, iterative 2D phase retrieval algorithms capable of retrieving both the phase and the amplitude of the pulse have been successfully implemented on this technique. The algorithm converges to a pulse that minimises the difference between the measured and simulated FROG traces.

An alternative method for measuring ultrashort laser pulses, called dispersion scan technique (d-scan), was invented in 2011 [12]. Unlike FROG and the autocorrelator, it does not rely on the measurement of the signal resulting from the temporal overlap between two pulses. Similar to them, the pulse to be measured is sent to a nonlinear medium where a nonlinear signal is generated, which is then spectrally resolved. The idea behind d-scan is the following. Nonlinear processes can be thought of as nonlinear functions acting on the pulse in the time domain. The amplitude in the time domain depends both on its corresponding spectral amplitude and on the spectral phase since the calculation to go from one domain to the other is done by means of the Fourier transform. Thus, in principle, if one is able to record the spectra while scanning the phase of the pulse, the resulting spectrogram should be sensitive to the spectral phase of the incident pulse.

To perform a phase scan, d-scan needs an experimental method that manipulates the spectral phase in a controlled way. Figure 2.14 shows a sketch of a SHG d-scan setup.
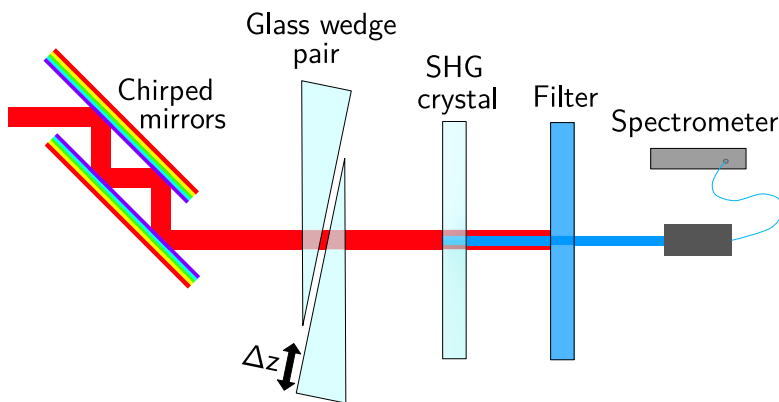

Figure 2.14: Simplified schematic of a d-scan setup.

As shown here, the method consists in transmitting the laser pulses through a glass wedge pair, one of which is mounted on a motorised translation stage. These add positive dispersion in the visible, mainly in the form of GDD although higher-orders will be more or less present depending on the material used. The amount of dispersion is also dependent on the thickness of the glass that the light has to pass through. For this reason, a simple way to perform the scan is to move one of the wedges and record the spectrum simultaneously.

Before the wedges, negative GDD is added to the pulse to ensure that, at the beginning of the measurement, the pulse is negatively chirped. Chirped mirrors, consisting of two highly reflective mirrors which act as a negative dispersive element, can be used for this purpose. Neglecting higher-order terms of dispersion (see Equation 2.38), for one certain material insertion the wedge pair compensates exactly for the negative GDD present in the pulse, thus flattening the spectral phase and making the pulses transform-limited. After the wedges, the high intensity pulses go through a nonlinear crystal where a harmonic signal, in the present case the second harmonic (SHG), is generated. Scanning (moving back and forth the wedge pair) around the point of optimal compression allows to record a 2D spectrogram with glass insertion on the vertical axis and frequency on the horizontal axis, which is known as the d-scan trace. To be able to retrieve the spectral phase, one needs to have a precise mathematical model describing the measurement of a d-scan. The evolution of the wave function as it goes through the setup is derived in the following. Initially, the pulse can be expressed in the frequency domain as:

$$\tilde{U}(\omega) = \left|\tilde{U}(\omega)\right| \exp\left[i\phi(\omega)\right] \tag{2.44}$$

After crossing the glass wedge pair, the pulse acquires a frequency dependent phase due to material dispersion that can be adjusted varying the amount of glass insertion, which is introduced here in the form of the variable z:

$$\tilde{U}(\omega, z) = \left|\tilde{U}(\omega)\right| \exp\left[i\phi(\omega)\right] \exp\left[ik_0 n(\omega)z\right] \tag{2.45}$$

Then SHG is performed. It can be modelled as a function that squares the electric field in the time domain:

$$U_{\text{SHG}}(t, z) = \left[\int \tilde{U}(\omega, z) \exp\left(i\omega t\right) d\omega\right]^2 \tag{2.46}$$

Finally, the spectrometer measures the spectral intensity $S(\omega, z)$ of the nonlinear signal.

$$S(\omega, z) = \left|\int U_{\text{SHG}}(t, z) \exp\left(-i\omega t\right) dt\right|^2 \tag{2.47}$$

It has been assumed in this model that the process of SHG can be described only as a squaring function of the electric field. This, however, is an ideal approximation since perfect phase-matching over the whole bandwidth of the pulse is needed for this to happen. A response function $R(\omega)$ is often included in the expression of the

spectrometer signal to compensate for the irregular spectral response [34]:

$$S_{\text{real}}(\omega, z) = R(\omega) S_{\text{ideal}}(\omega, z) \tag{2.48}$$

Simulating the d-scan trace of a predefined pulse is simple and provides a lot of information for the interpretation of measured d-scan traces of arbitrarily intricate pulse shapes. The result obtained after simulating the d-scan trace of a Gaussian pulse with an ideal full-width at half-maximum (FWHM) of 10 fs with a central wavelength of 800 nm is shown in Figure 2.15a. In this simulation, the wedges are considered to be made of BK7, whose refractive index as a function of frequency can be calculated from the Sellmeier equation. As can be seen here, the d-scan of a transform-limited pulse has the highest intensity at the position of zero glass insertion, in which the pulse does not acquire GDD and therefore it is maximally compressed. Moving up or down from this position, the intensity decreases due to the stretching of the pulse in the time domain. To simulate the d-scan trace of a pulse with spectral phase with higher-order terms, nonzero values must be introduced in the higher-order terms of the spectral phase polynomial expansion of the pulse (see Equation 2.38). As can be seen in Figure 2.15b, the simulated d-scan of a pulse with positive GDD is shifted mainly downwards and otherwise appears unaffected. The reason for this is that BK7 mainly contributes to the phase by adding positive GDD and therefore a negative insertion, i.e. glass removal, is needed to compensate for this and compress the pulse. When the pulse contains positive TOD, the trace appears to be tilted, as seen in Figure 2.15c. The last example, Figure 2.15d, shows that the presence of fourth-order dispersion (FOD) in the pulse gives a parabolic shape to the d-scan trace.
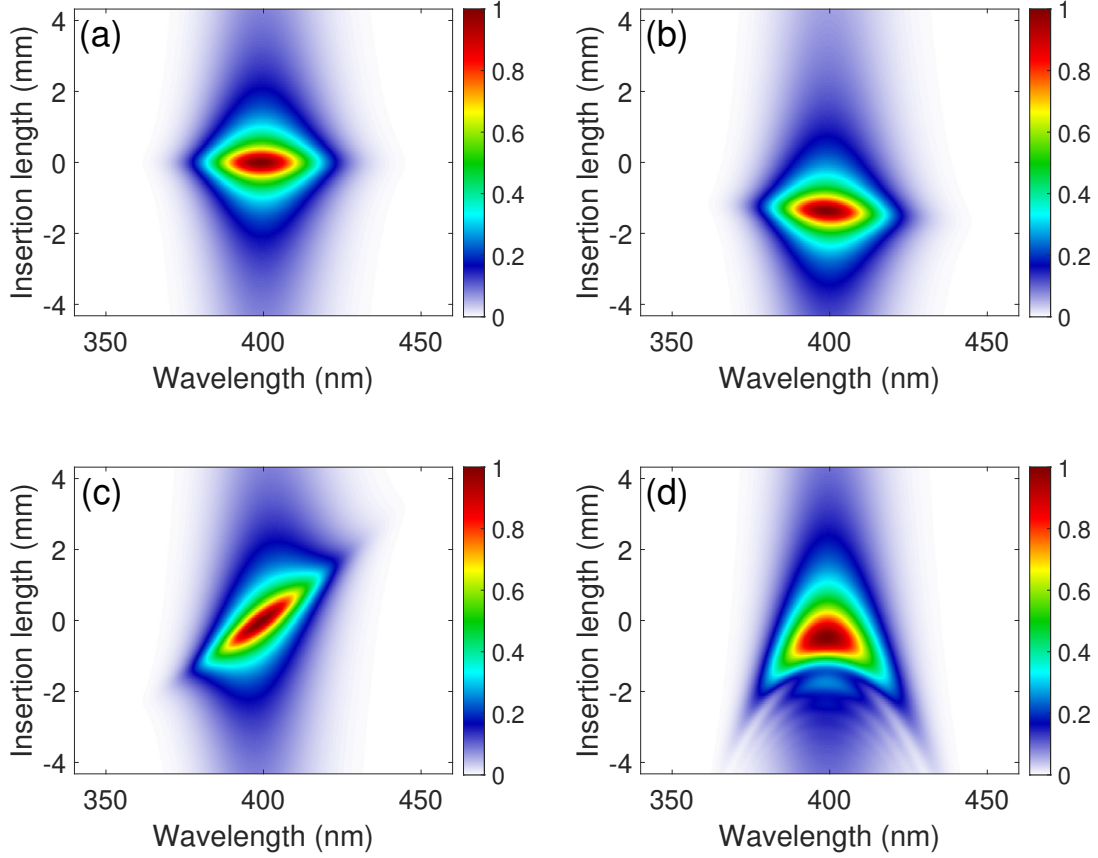
Figure 2.15: Simulated d-scan trace of a 10 fs Gaussian pulse for different spectral phase functions. (a) Zero spectral phase i.e the pulse is transform-limited. (b) Spectral phase with positive GDD. (c) Spectral phase with positive TOD. (d) Spectral phase with positive FOD.

These simulations clearly show that the d-scan technique is very sensitive to the spectral phase of the pulse, which is very important in order to retrieve it from the recorded spectrogram. In a similar way to FROG, a 2D phase retrieval algorithm is needed in order to retrieve the phase from the d-scan trace. The way this algorithm works is by, iteratively, trying to minimise the error between the simulated trace and the measured one. This error can be written as follows:

$$G^2 = \frac{1}{N_i N_j} \sum_{i,j} S_{\text{meas}}(\omega_i, z_j) - \mu S_{\text{sim}}(\omega_i, z_j) \tag{2.49}$$

Where μ is the factor that minimises the error and that has to be updated in every iteration:

$$\mu = \frac{\sum_{i,j} S_{\text{meas}}(\omega_i, z_j) S_{\text{sim}}(\omega_i, z_j)}{\sum_{i,j} S_{\text{sim}}^2(\omega_i, z_j)} \tag{2.50}$$

Solving optimisation problems, such as the one presented here, is a well-studied field of mathematics. A common method is least squares routines, such as the

Nelder-Mead algorithm. These have been successfully implemented in d-scan [36, 37]. Unfortunately, these methods tend to get stuck on local minima. A more recent approach has been to use a differential evolution-based algorithm [38], which appears to be less susceptible to stagnate at local minima. Another type of algorithms, commonly used in FROG, are the constraint-based inversion algorithms that have also been implemented in the d-scan technique [39]. In general, these algorithms converge to a solution faster than "brute force" ones based on least squares routines but have the disadvantage of being more sensitive to noise.

One of the strengths of d-scan is the simple in-line setup without the need of a reference pulse and interferometric precision, which makes the technique inherently more stable. Moreover, d-scan often manipulates dispersion using gratings or chirped mirrors, elements which are typically found in ultrafast laser compressor systems. This is a great advantage since it gives the possibility to compress and measure the laser pulses simultaneously. It is also important to mention that d-scan can be implemented using other nonlinear processes, such as third-order dispersion (TOD) d-scan [40], but one should keep in mind that higher-order nonlinearities generate much weaker signals.

Other pulse measurement techniques that do not require complex phase retrieval algorithms do exist. An example of these is spectral phase interferometry by direct reconstruction of the electric-field (SPIDER) [11], based on spectral interferometry between two pulse replicas that are shifted in frequency in respect to one another. These techniques, however, come at the expense of a much more complicated setup.

Chapter 3

Methods

The aim of this project is to include the measurement of a time-dependent polarisation state in the d-scan technique. This section deals with all the methods needed to implement this measurement, referred to in this work as polarisation d-scan. A first step is to devise a method capable of generating a predictable time-dependent polarisation state, which can serve as a proof of measurement. The method, detailed during the first part of this section, consists in transmitting linearly polarised light through a combination of two quarter-wave plates of different orders. After these elements, light has a polarisation state that changes as a function of time. This is known as polarisation gate. Simulations of the polarisation gate are made to serve as comparison with the final results.

As a guarantee that d-scan provides an accurate measurement of the polarisation gate, it is necessary that the elements used to generate it are properly characterised. The experimental method for its characterisation as well as its subsequent analysis is shown during the second part of this section, where an extensive study of wave plates is compiled, via calculations and experiments.

The third section of methods deals with both the experimental setup and the measurement procedure. The conventional d-scan setup needs to be redesigned and adapted to measure a time-dependent polarisation state. Furthermore, in this work a MATLAB script is developed to simulate the d-scan measurement of such a state in order to facilitate the evaluation of the final results.

3.1   Creating a Time-Dependent Polarisation State

3.1.1   Concept

To test the performance of the d-scan when measuring intricate vector pulses, a method capable of generating a predictable time-dependent polarisation state is needed. The approach used in this work to modulate the ellipticity of the femtosecond pulses consists in transmitting them through a combination of two wave plates, as it is illustrated in Figure 3.1.
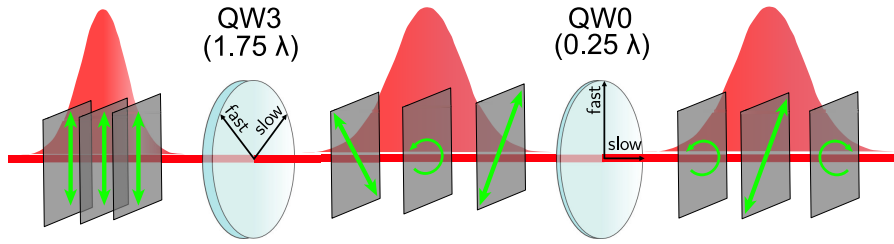
Figure 3.1: Schematic showing the generation of a time-dependent polarisation state, known as polarisation gate, by transmitting linearly polarised light through a combination of a third-order quarter-wave plate (QW3) and a zero-order quarter-wave plate (QW0). The green arrows represent the polarisation in planes perpendicular to the direction of propagation.

First, a linearly polarised pulse is sent through a third-order quarter-wave (1.75λ) plate, abbreviated as QW3, made of quartz and orientated such that its principal axes form an angle of 45° in respect to the incoming polarisation. This splits the incident pulse into two orthogonally polarised pulses with equal amplitudes whose directions of polarisation follow the principal axes of the wave plate. Each of these pulses propagates with a different speed due to the birefringent character, which originates a time delay as well as a dephasing of $7\pi/2$ between the fast axis polarised pulse and the slow axis polarised one. The time delay is such that the two pulses are separated in the time domain but leaving a time interval in the center during which they both overlap with a sufficiently high intensity. This condition limits the time delay to be less than the duration of the pulse. After the wave plate, the polarisation state changes as a function of time, going from linear polarisation (LP) at 135° to circular polarisation (CP) when both pulses have the same amplitude, and back to linear polarisation, this time at 45°.

Technically the first plate is enough to create the time-dependent polarisation state. However, for applications in the field of attosecond science it can be more useful to have a confined linear polarisation state in the middle of the pulse. To do this, the output pulse from QW3 is then transmitted through a zero-order quarter-wave (0.25λ) plate, abbreviated as QW0, also made of quartz and whose principal axes form an angle of 45° in respect to those of the higher-order plate. Again, the incoming pulse is split into two orthogonally polarised pulses that experience a small time delay and a dephasing of $\pi/2$. This converts linear polarisation to circular and vice versa. The combination of these two waveplates changes an input linear polarisation state into a time-varying polarisation pulse whose polarisation goes from left circular polarisation (LCP) to linear polarisation at 45° in the middle and back to right circular polarisation in the front (RCP).

3.1.2 Simulation of the Polarisation Gate

As discussed during section 2.1, there are different ways to describe a polarisation state and its evolution through polarisation sensitive elements like polarisers and wave plates. In Jones formalism, polarisation states are associated with vectors and

polarisation elements with matrix operators. Vectors, matrices, and their respective products can be easily implemented in a programming language like MATLAB. This allows the evolution of the polarisation state of light to be simulated as it propagates through an optical system. In particular, it can be used to simulate the polarisation gate. How this is done is detailed below:

A combination of two wave plates corresponding to two different orders of a quarter-wave plate can be used to generate a time-dependent polarisation state, referred to in this work as the polarisation gate. The Jones matrix of a quarter-wave plate of order M is shown in Equation 3.1:

$$\mathbf{M}_{\mathbf{QWM}}^{\text{achromatic}} = \begin{bmatrix} 1 & 0 \\ 0 & e^{i(2M+1)\pi/2} \end{bmatrix} \tag{3.1}$$

This matrix, however, represents a wave plate that adds the same relative phase shift regardless of wavelength, i.e. it assumes the plate to be achromatic. Although wave plates built for this purpose within a given wavelength range exist, the wave plates used in the experiments are designed for one wavelength. A more general matrix that can be used for chromatic wave plates is given in Equation 3.2:

$$\mathbf{M}_{\mathbf{QWM}}^{\text{chromatic}} = \begin{bmatrix} 1 & 0 \\ 0 & e^{i(2M+1)k_0[n_{\text{e}}(\nu)-n_{\text{o}}(\nu)]L_0} \end{bmatrix} \tag{3.2}$$

Here, the relative phase shift is expressed in terms of the wave vector (k), the ordinary $n_{\text{o}}(\nu)$ and extraordinary $n_{\text{e}}(\nu)$ refractive indices, and the zero-order thickness of the crystal (L_0).

The first step in the simulation is to define a vector that corresponds to linearly polarised light in the vertical direction. Equation 3.3 shows the formula used for this:

$$\tilde{\mathbf{J}}_{\mathbf{i}}(\boldsymbol{\nu}) = A(\boldsymbol{\nu}) \cdot \begin{bmatrix} 0 \\ 1 \end{bmatrix} \tag{3.3}$$

Here, the Jones vector is multiplied by a factor $A(\boldsymbol{\nu})$, which represents the spectral amplitude of the light before it passes through the wave plates. Therefore, the Jones vector used in the simulations is not a vector but a matrix of dimension $2 \times N$, where N is the number of frequency points needed to simulate the spectrum of the incoming pulse. For simplicity, the factor $A(\boldsymbol{\nu})$ is calculated assuming a Gaussian-shaped pulse with temporal width Δt and central frequency ν_0. In Equation 3.4 the formula used for this purpose is shown:

$$A(\boldsymbol{\nu}) = \exp\left[-\pi^2 \Delta t^2 \left(\boldsymbol{\nu} - \nu_0\right)^2\right] \tag{3.4}$$

The evolution of the Jones vector through the combination of wave plates is calculated using matrix multiplication, as shown in Equation 3.5:

$$\tilde{\mathbf{J}}_{\mathbf{f}} = \mathbf{M}_{\mathbf{QW0}} \times \mathbf{R}(-45°) \times \mathbf{M}_{\mathbf{QW3}} \times \mathbf{R}(45°) \times \tilde{\mathbf{J}}_{\mathbf{i}} \tag{3.5}$$

The Jones vector in the time domain can be calculated applying the Fourier transform over the Jones vector in the frequency domain, as shown in Equation 3.6:

$$\mathbf{J_f(t)} = \mathcal{F}\left\{(\tilde{\mathbf{J}}_\mathbf{f}(\boldsymbol{\nu})\right\} \tag{3.6}$$

The new form of the Jones vector is shown in Equation 3.7:

$$\mathbf{J_i(t)} = \begin{bmatrix} A_x(\mathbf{t})\,e^{i\varphi_x(\mathbf{t})} \\ A_y(\mathbf{t})\,e^{i\varphi_y(\mathbf{t})} \end{bmatrix} \tag{3.7}$$

The amplitude ratio and the relative phase difference between two orthogonal components of the electric field can be calculated as a function of time from the Jones vector. In other words, it describes the polarisation state of light as a function of time. This can be visualised graphically by calculating the angle of ellipticity (χ) at each time using Equation 2.15 and plotting it as function of time. Figure 3.2 shows the result of a simulation where a 6 fs pulse with a central frequency of 0.375 PHz (800 nm) is transmitted through the combination of wave plates. This figure shows the angle of ellipticity as a function of time after the wave plates, along with the resulting pulse envelope:
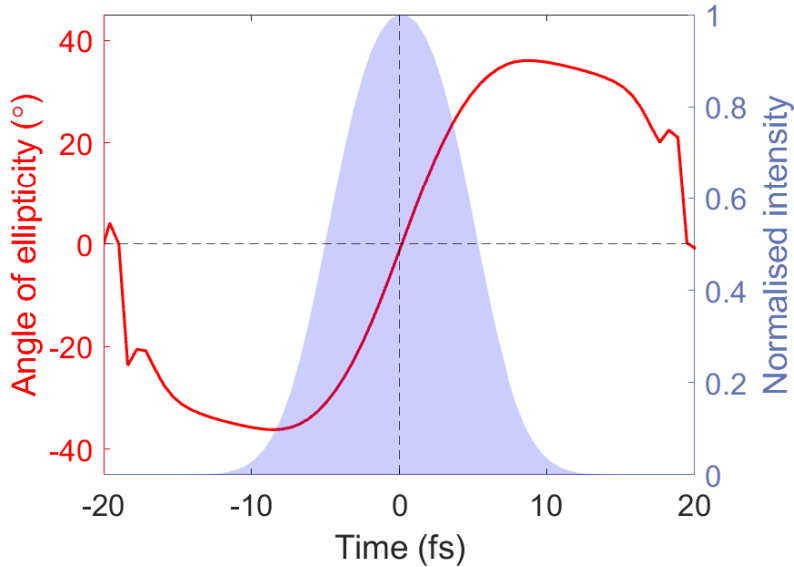

Figure 3.2: Simulation of the polarisation gate. The angle of ellipticity of the electric field after the combination of wave plates is plotted as a function of time. In addition to this, the shaded area represents the envelope of the polarisation gate pulse.

The temporal width of the pulse has increased due to the effect of the wave plates. At the beginning of the pulse (negative time), the ellipticity angle has a value of $\chi \approx -40°$. It decreases rapidly, crossing $\chi = 0°$ in the middle of the pulse, and reaches a value of $\chi \approx +40°$ on the opposite side of the pulse (positive time). In terms of polarisation states, the pulse starts left circularly polarised, becomes linearly polarised in the middle, and is right circularly polarised at the end.

It is also interesting to look at the intensity for different projections of the electric field, specially those at 45° and 135°. As shown in Equation 3.8, first the Jones vector is multiplied by a rotation matrix of 45° so that the axes of the new reference frame are aligned with the directions at 45° and 135°.

$$\mathbf{J'_f} = \mathbf{R}(45°) \times \mathbf{J_f} \tag{3.8}$$

To calculate the electric field intensity for these two projections, the Jones vector is first projected in each of the two orthogonal directions of the new reference frame and then squared. Mathematically this is implemented using Equations 3.9 and 3.10:

$$I(45°) = \left| \begin{bmatrix} 1 & 0 \end{bmatrix} \times \mathbf{J'_f} \right|^2 \tag{3.9}$$

$$I(135°) = \left| \begin{bmatrix} 0 & 1 \end{bmatrix} \times \mathbf{J'_f} \right|^2 \tag{3.10}$$

Figure 3.3 shows the results of these calculations. As seen in this figure, the intensity of the projection at 45° follows a Gaussian distribution, slightly broader than the input pulse and with about half the maximum intensity. In addition, the intensity distribution of the projection at 135° exhibits a double peak structure with less than a quarter of the intensity of the input pulse. The explanation for this lies in the time-dependent polarisation state. According to the model presented in the previous section and then verified by ellipticity angle calculation, the polarisation gate should have linear polarisation at 45° in the middle of the pulse. Projecting the electric field at 135° should completely cancel the intensity in the middle of the pulse, which is observed in this calculation.
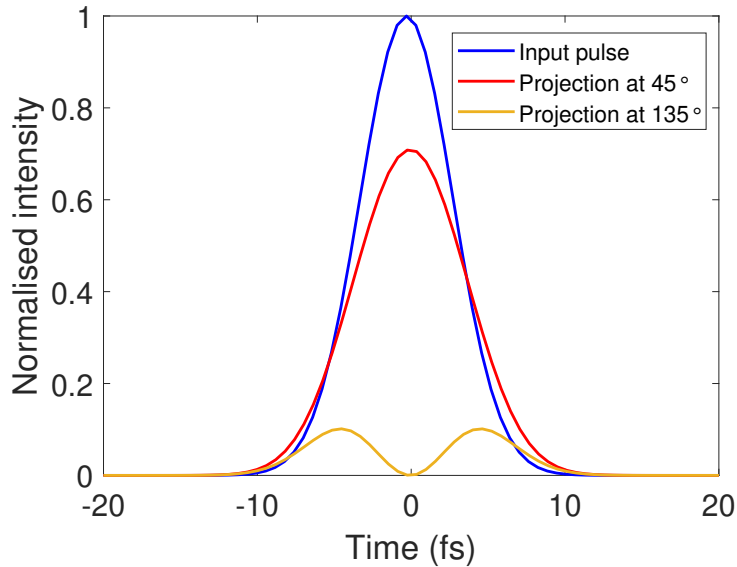

Figure 3.3: Simulation of the polarisation gate. The envelopes of the input pulse and the two linearly polarised projections at 45° and 135° after the combination of the two wave plates are plotted.

3.2   Characterisation of Wave Plates

As seen in Equation 2.9, the relative phase shift added by a wave plate depends on wavelength. For this reason, wave plates are typically built for a central wavelength (λ_0) and their effect on the polarisation state departs from ideal behavior as soon as the wavelength of light becomes different. In principle, one should expect the rate of change of the polarisation state after the wave plate as a function of wavelength to increase with wave plate order, since higher orders add more relative phase for a given wavelength, as seen in Equation 3.1. To ensure that the wave plates used in the experiments are the correct ones, a setup for their characterisation was mounted in the lab.

A common method to characterise the function of a wave plate is to place it between two polarisers, illuminate it with a broadband light source and spectrally resolve the intensity with a spectrometer. The idea behind this configuration is as follows. The first polariser is fixed in a given orientation and linearly polarises the incident light in that direction. The light then passes through the wave plate to be characterised, resulting in a change of the polarisation state. The polariser located after the plate plays the role of the "analyser". During the characterisation process, measurements are taken as the analyser is rotated, in order to measure the spectral intensity corresponding to different projections of the electric field. For this kind of experiments, broadband light sources such as a white incandescent lamp are typically used [41]. Instead, in this work ultrashort laser pulses coming directly from the oscillator are used for illumination. These pulses have a wide bandwidth in the spectral range where the wave plates are used during the experiments, making them a great tool for their characterisation. Figure 3.4 shows a sketch of the setup used in the lab for this purpose:
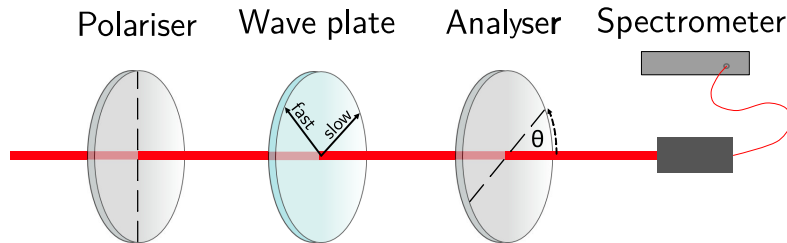

Figure 3.4: Simplified schematic of the wave plate characterisation setup.

Before starting the characterisation, one needs to locate the principal axes of the wave plate. The first step is to set the two polarisers to be cross-polarised by rotating the second polariser until the measured intensity is at a minimum. Then, the wave plate is inserted in between them. One of the principal axes of the wave plate is aligned with the polarisation axis of the first polariser when the measured intensity remains minimum. The reason for this is that in this position the electric field only acquires an absolute phase and this has no effect on the polarisation state. A measurement of the laser spectrum is needed to normalise the measurements. This is done by measuring the spectrum when the two polarisers are parallel and one of the wave plate principal axes is aligned with the input polarisation.

To start the characterisation, the wave plate is orientated at 45° relative to the input polarisation. The initial position of the analyser is cross-polarised in respect to the first polariser. As a measurement convention, an analyser angle of 0° corresponds to the initial position, where its polarisation axis is aligned with the horizontal direction. Intensity is recorded every 10° as the analyser is rotated from 0° to 180°, which corresponds to one complete revolution of its polarisation axis.

A simulation of the wave plate characterisation can also be implemented with MAT-LAB. Similar to the polarisation gate simulation, which was described in subsection 3.1.2, the evolution of the Jones vector through the setup is computed using matrix multiplication, as shown in Equation 3.11:

$$\tilde{\mathbf{J}}_\mathbf{f}(\boldsymbol{\nu}, \boldsymbol{\theta}) = \mathbf{R}(\boldsymbol{\theta}) \times \mathbf{R}(-45°) \times \mathbf{M_{QW}} \times \mathbf{R}(45°) \times \tilde{\mathbf{J}}_\mathbf{i}(\boldsymbol{\nu}) \tag{3.11}$$

The final Jones vector is evaluated for an array of frequencies ($\boldsymbol{\nu}$) in order to simulate the data points measured by the spectrometer as well as for an array of angles ($\boldsymbol{\theta}$) that simulates the different projections of the analyser.

The two quarter-wave plates used in the experiments to generate the polarisation gate, QW0 and QW3, are characterised via simulations and measurements. In both cases, the collected data can be arranged in a matrix form with 19×2838 data points (2838 is the number of frequency points measured by the spectrometer). The spectra obtained for each wavelength is normalised by the intensity of the input laser at that wavelength. The resulting image of plotting this matrix for both simulations and measurements is shown in Figure 3.5. Each pixel in these images has a value that corresponds to the intensity of light for each wavelength and angle of the analyser, which is represented in the color map.
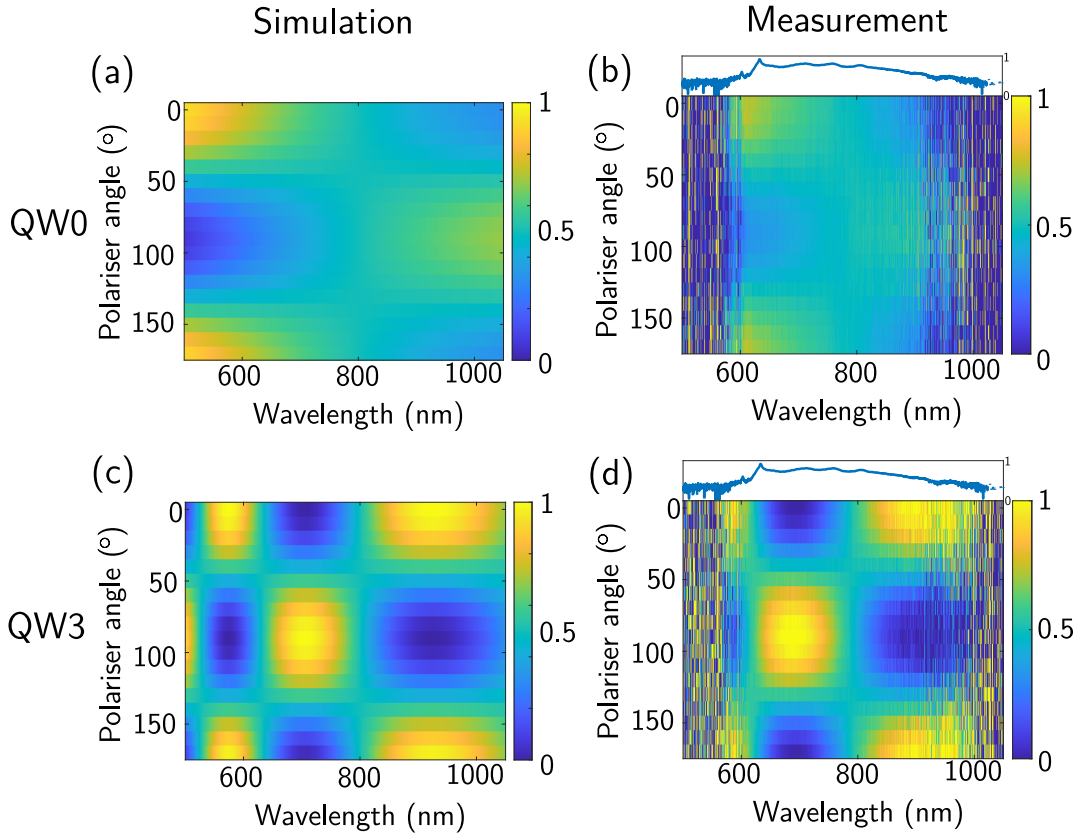
Figure 3.5: 2D plot for wave plate characterisation. (a)-(b) Measurements and simulation of the zero-order quarter-wave plate (QW0). (c)-(d) Measurements and simulation of the third-order quarter-wave plate (QW3). The input laser spectrum is represented in logarithmic scale on top of the measured spectrograms.

As seen in Figures 3.5b and 3.5d the signal to noise ratio (SNR) is good inside the wavelength range between approximately 620 nm and 900 nm which, as seen on top of these images, correspond to the limits of the laser spectrum. Outside this wavelength range the SNR clearly drops because fluctuations in laser intensity become as significant as the laser intensity itself. Besides this, there is a good agreement between simulations and measurements in both cases. From these images it is possible to determine the polarisation state of light for different wavelengths. This can be done by measuring for each wavelength the contrast between the regions of higher and lower intensity of the image as a function of the angle of the analyser. While high contrast indicates that the polarisation state is linear for that wavelength, low contrast indicates that light is circularly polarised. This characterisation shows that both wave plates are built for a central wavelength of 800 nm, since exactly at this wavelength the contrast is very low and thus the polarisation state is circular. As soon as the wavelength departs from this value the intensity begins to depend on the analyser angle, meaning that the state of polarisation after the wave plate is no longer circular. Additionally, one can also see that the rate of change of the polarisation state as a function of wavelength is significantly higher for the higher-order wave plate, which was expected.

For each wavelength, the measurements of intensity as a function of analyser angle

can be fitted to an oscillating function. This is chosen to be an extended version, i.e. with more degrees of freedom, of Malus's law, as shown in Equation 3.12:

$$I(\theta) = a + b\cos^2(\theta + c) \tag{3.12}$$

Figure 3.6 shows the result of making this fit for both wave plates. Although the fit has been made for all the wavelengths data sets (2838), only the results obtained for 10 wavelengths that are approximately spaced by 60 nm around a wavelength of 800 nm are shown here:
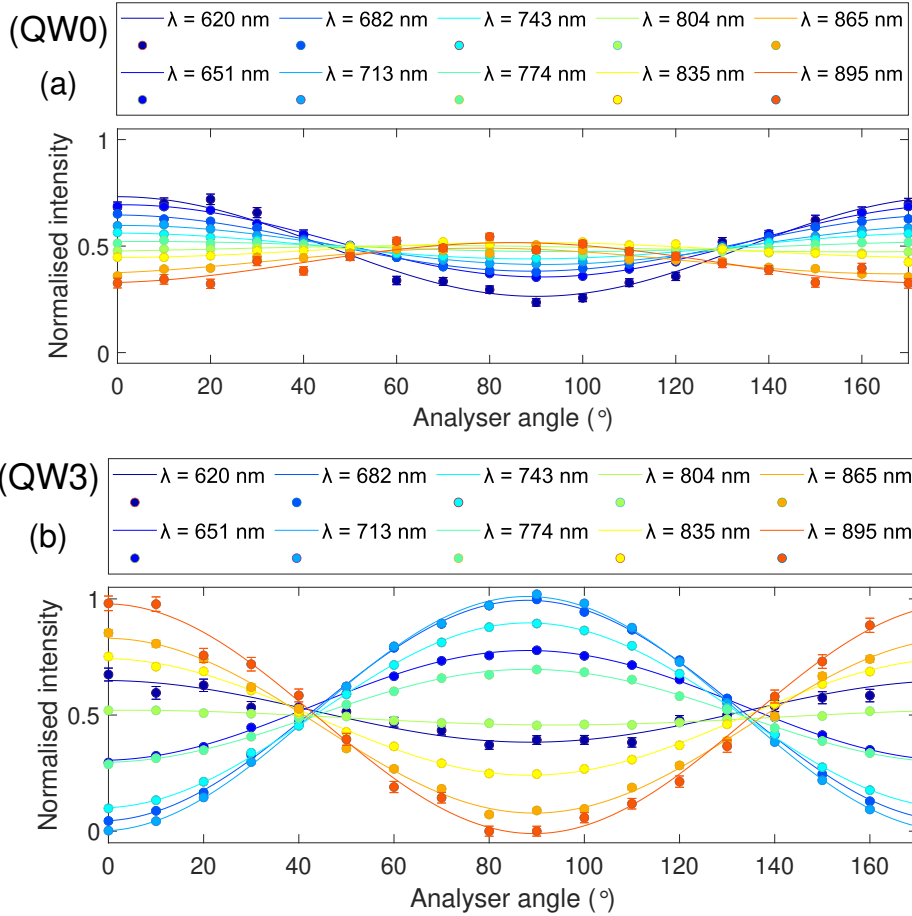

Figure 3.6: Normalised measured intensity as a function of the analyser angle. (a) Zero-order quarter-wave plate (QW0). (b) Third-order quarter-wave plate (QW3).

From the fit parameters, the intensity for two orthogonal directions, I_x and I_y, as well as the relative phase difference between them, φ, can be easily calculated. Next, using the equations 2.14 and 2.15 the orientation (ψ) and ellipticity (χ) angles can be calculated. Finally, these angles can be plugged into Equations 2.16, 2.17, 2.18 and 2.19 in order to calculate the Stokes parameters . As seen during subsection 2.1.3, these correspond to the coordinates of a polarisation state on the Poincaré sphere. Figure 3.7 shows the results obtained after plotting the polarisation states calculated from the simulations and measurements using the Poincaré sphere representation:
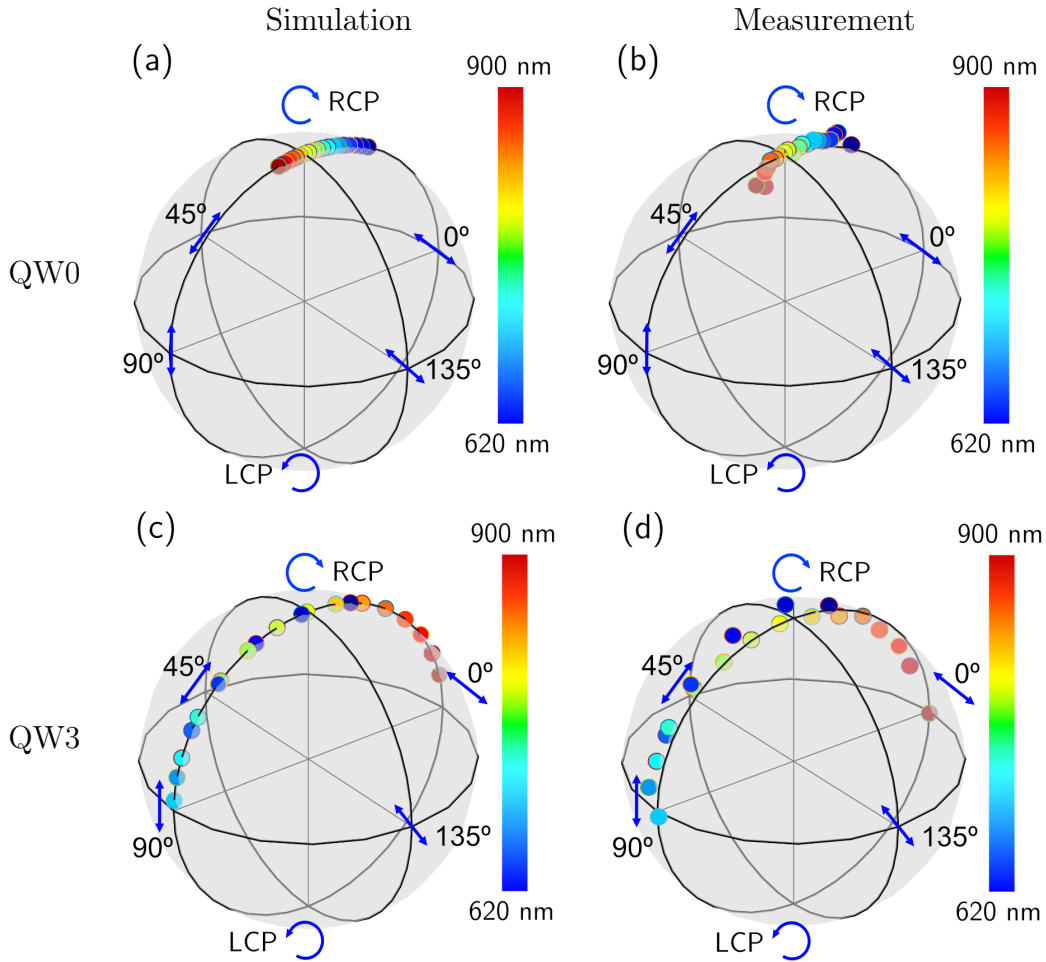
Figure 3.7: Representation of the state of polarisation using the Poincaré sphere for a total of 20 wavelengths between 620 nm and 900 nm. (a)-(b) Measurements and simulations of QW0. (c)-(d) Measurements and simulations of QW3.

This representation serves to visualise clearly how the polarisation state changes as a function of wavelength for each wave plate. For QW0, Figures the 3.7a and 3.7b show that all points are close to the top vertex of the sphere, meaning that even for a wide wavelength range of 280 nm light exhibits approximately circular polarisation. Instead, Figures 3.7c and 3.7d show that polarisation changes quickly after QW3, going from circular polarisation at 620 nm to linear polarisation at 700 nm, circular at 800 nm and finally linear at 900 nm. As seen in the results from the simulations, Figures 3.7a and 3.7c, all states of polarisation lie exactly on the surface of the Poincaré sphere. This is not the case in the results obtained from the measurements, Figures 3.7b and 3.7d, where the states of longer wavelengths (red colors) tend to go under the sphere while shorter wavelengths (blue colors) above the sphere. Measurements were normalised by the spectrum measured when one of the wave plates principal axes is aligned with the input polarisation. A small error in this alignment could have been the cause of the discrepancy in the radial coordinate of the measured polarisation states.

3.3 Measurement of a Polarisation D-Scan

This section aims to provide a description of the experimental setup, the measurement method and a model to perform simulations of the measurements using MATLAB.

3.3.1 The Experimental Setup

In this segment, the experimental setup designed and built for measurement of a time-dependent polarisation state with d-scan is described in detail. The experimental design is fundamentally based on the idea of a conventional d-scan, which has been presented during subsection 2.3.3 and represented schematically in Figure 2.14.

In the experiments performed during this work, a Titanium-Sapphire ultrafast oscillator delivers ultrashort laser pulses with a duration of 6 fs FWHM at a carrier wavelength of approximately 850 nm and with a repetition rate of 80 MHz [42]. In a second stage, which consists of an optical parameter chirp pulse amplification (OPCPA) system, the pulses emitted by the oscillator are amplified up to an average power of 3 W and the repetition rate is reduced to 200 KHz [42]. The d-scan setup is located in line with the output of the OPCPA system. Between the OPCPA and the d-scan setup is a beam shutter to let in or block out light when needed. A measurement of the laser spectrum is shown in Figure 3.8:
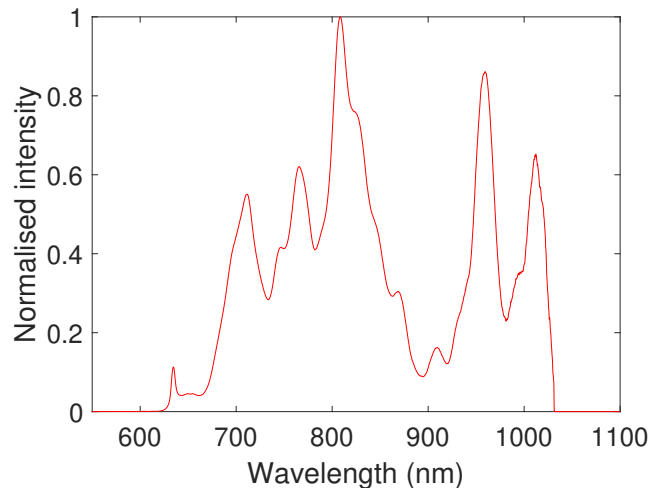
Figure 3.8: Measured spectrum of the laser.

A drawing of the experimental setup is presented in Figure 3.9. This configuration has two different functions. On the one hand, the conventional design of the d-scan technique is adapted to measure linearly polarised projections of the electric field. On the other hand, the assembly includes the optical elements that are necessary for the generation of the polarisation gate. A description of the role of the different elements is presented below:

Chirped mirrors (CMs) are used to add negative chirp to the pulses. These are part of the pulse compression system at the output of the OPCPA. Further down in the beam path there is a wedge pair made of BK7 glass which, as oppose to the CMs, is responsible for adding positive chirp. One of the wedges is mounted on a motorised translation stage so as to scan the amount of glass that light has to pass through. The iris located after the wedges is used simply to provide the ability to manually decrease the power of the beam, which may be necessary to avoid saturating the fiber coupled collector (D2) or for alignment purposes. A flat mirror (M1) and a spherical mirror with a long focal length (M2) are used to reorient and align the beam path.
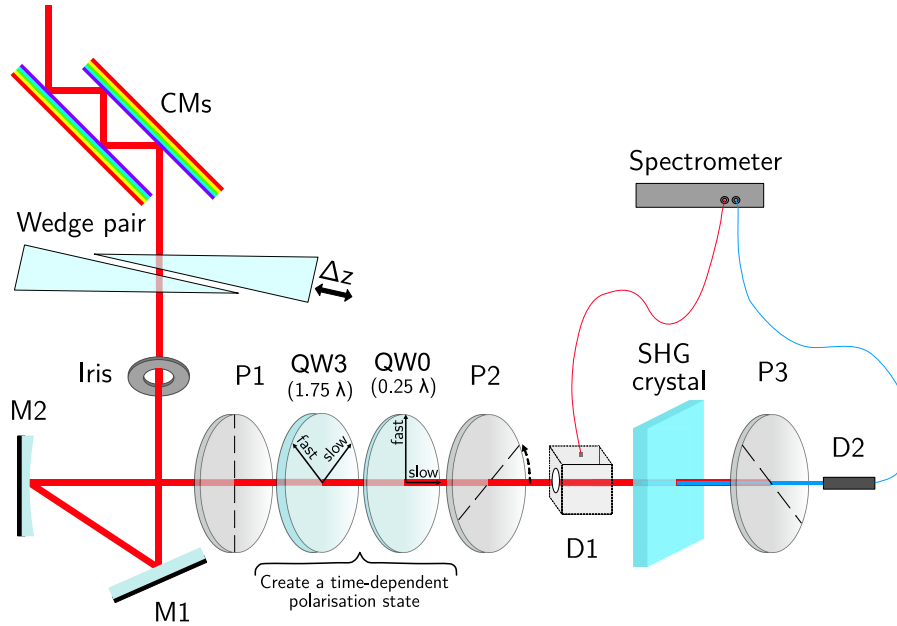

Figure 3.9: Schematic of the polarisation d-scan setup.

The elements needed to generate the polarisation gate are now introduced. Although in principle the laser pulses are vertically polarised, the first element along this line is a linear polariser (P1) which is used to obtain a "clean" linear polarisation state. Once the polarisation has been cleaned, a combination of two quarter-wave plates converts the linear polarisation into a time-dependent polarisation state, known as the polarisation gate. This method has been explained during Section 3.1.

A second linear polariser (P2) is used to project the electric field of the pulses in a certain direction which can be turned by rotating the polariser. A BBO crystal is precisely placed in the focal plane of M2, where the laser intensity is highest, to generate the second harmonic through SHG. Two orientations of the SHG crystal relative to the incident polarisation maximise the intensity of the second harmonic signal, the explanation is as follows. Because ooe phase matching takes place in the BBO crystal (see subsection 2.2.2), the intensity of the second harmonic is maximised when the polarisation of the incident laser beam aligns with the ordinary direction in the crystal. In a 360° rotation this condition is met twice, due to the 180° rotation symmetry. In the experimental setup, the SHG crystal is mounted on a rotation mount to rotate it to find the orientation for which the nonlinear signal is

maximised. A third polariser (P3) is oriented perpendicular (cross-polarised) to the second polariser (P2) to cancel the fundamental radiation as well as the residual second harmonic that might be present before the SHG crystal.

As seen in this setup, two devices are used to collect light and transmit it to the spectrometer: an integrating sphere (D1) and a fiber coupled collector (D2), which have different roles in the measurement process. The integrating sphere consists of a spherical diffusing cavity that is attached to a fiber. This is placed after the second polariser and must be manually removed when not needed. The fiber coupled collector is fixed to the optical table and it is located after the third polariser. Due to its higher sensitivity, it is used to collect the nonlinear signal generated in the SHG crystal. As opposed to the large aperture area of the integrating sphere, it has a very small effective area, requiring a careful alignment. Both instruments collect light and transmit their signals to a fiber-coupled spectrometer (Avantes) that can operate in the spectral range between 200 nm and 1100 nm.

Compared to a conventional d-scan setup, this setup allows reconstruction of linearly polarised pulses corresponding to different projections of the electric field. As mentioned above, one of the complexities of these measurements is that the SHG crystal must be rotated each time the second polariser is rotated due to the need to maximise the efficiency of second harmonic generation. Similarly, the third polariser must remain cross-polarised and therefore must be rotated when the second is rotated and by the same amount. A schematic description of the measurement procedure is detailed below.

3.3.2   Measurement Procedure

Before starting to measure, it is necessary to calibrate the wave plates and the polarisers so as to find their initial orientations. Polariser 1 can be set at any angle whereas polariser 2 determines the angle of the linearly polarised projection. To do so, the following steps are followed:

1. The integrating sphere is placed after polariser 2 and connected to the spectrometer.

2. Polariser 1 is added to the setup with an arbitrary orientation.

3. Polariser 2 is added to the setup. By turning this polariser we look for the position at which the intensity recorded with the spectrometer reaches a minimum. Here polariser 2 is cross-polarised with respect to polariser 1. This position corresponds to an angle of $0°$.

As for the wave plates, QW3 must be oriented so that its principal axes form an angle of $45°$ with respect to the incoming polarisation, set by the polarisation axis of P1. This ensures that when light hits the wave plate, the amplitude of the electric field is split equally between the two principal directions. On the other hand, QW0 must be oriented such that its principal axes form an angle of $45°$ with respect to those of QW3, meaning that one of the principal axes is aligned with the polarisation axis

of P1. Each wave plate is calibrated separately and then recombined in the setup with their new orientations. How to locate the principal axes of a wave plate has already been explained in section 3.2.

To perform the d-scan measurement for a linearly polarised projection of the electric field defined by the orientation of polariser 2, one needs to follow a series of steps:

1. The beam shutter is closed. The integrating sphere is inserted after polariser 2. The recorded spectrum is saved as a background to be subtracted from subsequent measurements.

2. The shutter opens again. The iris opens fully for maximum laser power. The spectrum is measured and saved as the fundamental spectrum.

3. The iris closes completely. The integrating sphere is removed from the setup. The iris is adjusted until the intensity measured with the fiber detector reaches a high enough value without saturating.

4. Polariser 3 is now added to the setup. Rotating polariser 3, we look for the position where the intensity reaches a minimum. Here polariser 3 is cross-polarised with respect to polariser 2.

5. The SHG crystal is added to the setup, in a position that would ideally correspond to the focal plane. Rotating the SHG crystal we look for the position at which the second harmonic signal is maximised while the fundamental is minimised.

6. The nonlinear signal is optimised by finely opening the iris, without reaching saturation. Now, we proceed to measure the spectrum while scanning the position of the wedge around the point of optimal compression. The resulting spectrogram constitutes the measured d-scan trace for the projection of choice.

7. The same procedure must be repeated again for a different projection.

The measurements are then processed with a software developed for the d-scan technique. This program uses the measured d-scan trace together with the fundamental spectrum to retrieve the spectral phase of the pulse. The program uses the fundamental spectrum to make an initial guess of the spectral phase. By simulating the d-scan trace for that spectral phase, the program obtains a parameter that reflects the difference between the measured trace and the simulated one. Through a series of iterations, the algorithm is able to find a spectral phase that minimises such parameter and converges to a solution. From this solution, the program calculates the Fourier transform and reconstructs the pulse profile in the time domain.

3.3.3 Simulation of a Polarisation D-Scan

The problem of simulating a polarisation sensitive d-scan trace can be reduced to being able to simulate two different effects caused by the propagation of the pulses

through the optical system, one is the evolution of the polarisation state and the other is the effect of dispersion on the complex amplitude of the pulses.

How to model polarisation has already been explained during subsection 3.1.2. Dispersion is modeled in the simulations considering only the effect of material dispersion. The refractive index is simply calculated from the Sellmeier equation of the material in question and evaluated on a specific array of frequencies ($\boldsymbol{\nu}$), used to simulate the spectrum of the laser. these values are used to calculate the acquired spectral phase using Equation 2.40. To calculate the dispersion added by the wedge pair as a function of glass insertion, an array of glass insertion points ($\mathbf{z}$) is created and included in the calculation of the spectral phase. This yields a two-dimensional matrix, where each value represents the spectral phase for a given value of frequency and glass insertion. The precise formula used for this calculation is written in Equation 3.13.

$$\psi(\boldsymbol{\nu}, \mathbf{z}) = \frac{2\pi\nu}{c_0} n(\boldsymbol{\nu}) \times \mathbf{z} \tag{3.13}$$

A general expression for the Jones vector is shown in Equation 3.14. In the simulation this is not treated as a vector but as $2 \times$ N $\times$ P matrix where N and P correspond to the number of simulated frequency and glass insertion points, respectively.

$$\tilde{\mathbf{J}}(\boldsymbol{\nu}, \mathbf{z}) = \begin{bmatrix} E_x(\boldsymbol{\nu}, \mathbf{z}) \\ E_y(\boldsymbol{\nu}, \mathbf{z}) \end{bmatrix} \tag{3.14}$$

Linearly polarised light is simulated by setting to zero one of the components of the Jones Vector, as shown in Equation 3.15. Here, the complex electric field is expressed in the frequency domain and calculated as the product between a real spectral amplitude $A(\boldsymbol{\nu},\mathbf{z})$ that gives shape to the pulse and a spectral phase $\psi(\boldsymbol{\nu},\mathbf{z})$.

$$\tilde{\mathbf{J}}_{\mathbf{i}}(\boldsymbol{\nu}, \mathbf{z}) = \begin{bmatrix} 0 \\ A(\boldsymbol{\nu}, \mathbf{z})\, e^{i\psi(\boldsymbol{\nu}, \mathbf{z})} \end{bmatrix} \tag{3.15}$$

The evolution of the Jones vector as light propagates through the wave plates is computed using matrix multiplication, as shown in Equation 3.16. Here, the rotation matrix $\mathbf{R}(\theta)$ is included in order to be able to rotate the reference frame and thus be able to project the electric field in any direction.

$$\tilde{\mathbf{J}}_{\mathbf{f}} = \mathbf{R}(\theta) \times \mathbf{M}_{\mathbf{QW0}} \times \mathbf{R}(-45°) \times \mathbf{M}_{\mathbf{QW3}} \times \mathbf{R}(45°) \times \tilde{\mathbf{J}}_{\mathbf{i}} \tag{3.16}$$

The corresponding Jones vector in the time domain can be calculated making the Fourier transform of the Jones vector in the frequency domain.

$$\mathbf{J}_{\mathbf{f}}(\mathbf{t}, \mathbf{z}) = \mathcal{F}\left\{ (\tilde{\mathbf{J}}_{\mathbf{f}}(\boldsymbol{\nu}, \mathbf{z}) \right\} \tag{3.17}$$

As shown in Equation 3.18, now the amplitude and phase are time-dependent.

$$\tilde{\mathbf{J}}_{\mathbf{i}}(\mathbf{t}, \mathbf{z}) = \begin{bmatrix} A_x(\mathbf{t}, \mathbf{z})\, e^{i\varphi_x(\mathbf{t}, \mathbf{z})} \\ A_y(\mathbf{t}, \mathbf{z})\, e^{i\varphi_y(\mathbf{t}, \mathbf{z})} \end{bmatrix} \tag{3.18}$$

The generation of the second harmonic is calculated squaring the complex electric field in the time domain. To go back to to frequency domain the inverse Fourier transform is applied over the complex amplitude of the SHG signal.

$$\tilde{\mathbf{J}}_{\mathbf{SHG}}(\boldsymbol{\nu}, \mathbf{z}) = \mathcal{F}^{-1}\left\{ \left[(\mathbf{J}_{\mathbf{f}}(\mathbf{t}, \mathbf{z}))^2 \right] \right\} \tag{3.19}$$

Finally, the second-harmonic multidimensional Jones vector is converted to a two-dimensional matrix $S(\boldsymbol{\nu}, \mathbf{z})$ after projecting it in one of the two orthogonal directions. Then each value in this matrix is squared to calculate the intensity of the nonlinear signal. An image plot of this matrix corresponds to the simulation of the measured d-scan trace for a given projection of the electric field.

$$S_{x,y}(\boldsymbol{\nu}, \mathbf{z}) = |\mathbf{J}_{\mathbf{x,y}} \times \tilde{\mathbf{J}}_{\mathbf{SHG}}(\boldsymbol{\nu}, \mathbf{z})|^2 \tag{3.20}$$

The developed MATLAB code allows simulating a d-scan measurement for any projection of the electric field, producing a simulated d-scan trace. In addition to this, the code allows the possibility of adding any pulse shape, from a simple Gaussian shape to importing the spectrum measured during the experiments, as well as changing the type of material from which the optical elements are made. An example code of the polarisation d-scan simulation can be found in Appendix A.

Chapter 4

Results and Discussion

The objective of this section is to present and discuss the main results obtained during the realisation of this project. It is divided into three parts consisting of the polarisation gate characterisation, d-scan measurements and reconstruction of the electric field.

A continuation of the wave plate characterisation presented during section 3.2 is the characterisation of the combination of wave plates used to generate the polarisation gate. The results of this are shown during the first part of this section.

The d-scan measurements of four linearly polarised projections of the electric field are presented during the second part. For comparison, these measurements are accompanied by their respective simulations as well as the retrieved d-scans.

The third part of this section deals with the method used to go from experimental results to reconstructing the electric field. Each of the steps is accompanied by representative figures. In the last segment, a figure showing the reconstruction of the electric field is presented.

4.1 Characterisation of the Polarisation Gate

Figure 4.1 shows the 2D characterisation plot of the polarisation gate. A good agreement between the simulation and the measurements is observed. In this figure, a high intensity contrast is observed as a function of the polariser angle throughout the entire represented spectrum. This serves as an indication that the polarisation state associated with each of these wavelengths is approximately linear. It is also observed that the position of the intensity maximum shifts at different angles of the polariser when measuring different wavelengths. This indicates that the direction of the polarisation state rotates with wavelength.
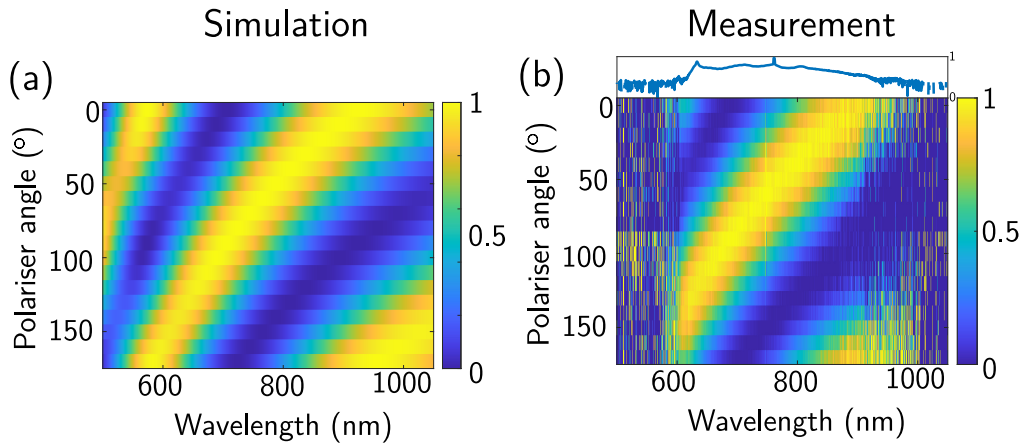
Figure 4.1: Characterisation of the polarisation gate. 2D plot showing the value of intensity as a function of analyser angle and wavelength. (a) Simulation. (b) Measurement.

In Figure 4.2 the state the polarisation state for different wavelengths is plotted on the Poincaré sphere. Except for the shortest wavelengths, around 620 nm, which exhibit elliptical polarisation states, all other wavelengths have a polarisation state located near the equator of the sphere, which means they are linearly polarised. It is also observed that the linear polarisation changes direction rapidly since it goes from 90° for short wavelengths to 0° for the longest ones.
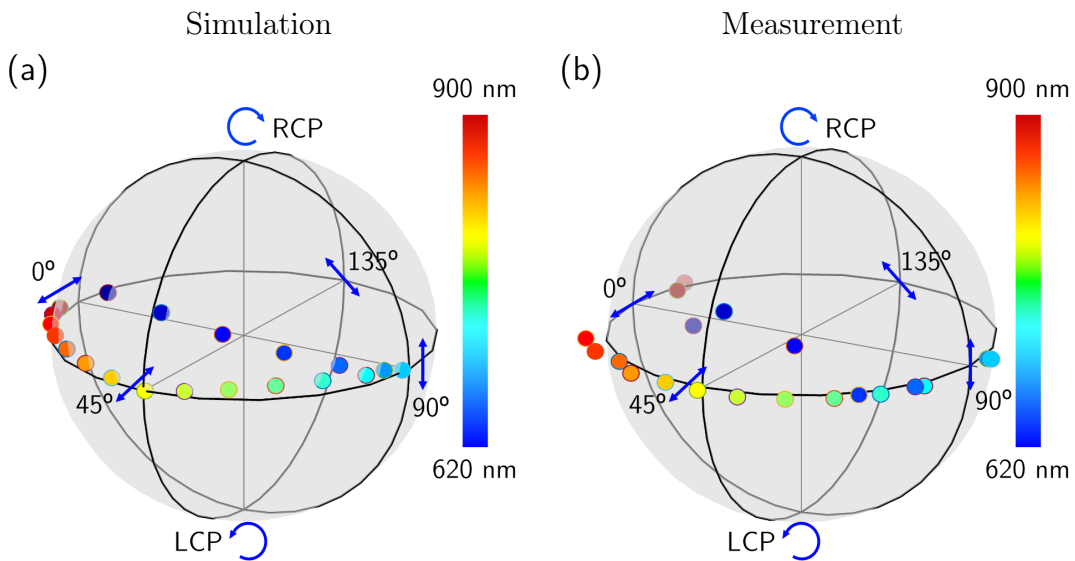

Figure 4.2: Characterisation of the polarisation gate. The state of polarisation for a total of 20 wavelengths between 620 nm and 900 nm is represented using the Poincaré sphere. (a) Simulation. (b) Measurement.

4.2 D-Scan of the Polarisation Gate

Figure 4.3 shows the measured d-scan trace of the input pulse, together with its simulation and retrieval, when no time-dependent polarisation is induced in the pulses. This is achieved by aligning the two wave plates with the initial polarisation direction so that the polarisation state of the laser is not affected when passing through them. This measurement provides the laser pulse parameters on the measurement day, as these ones are subject to change from day to day.
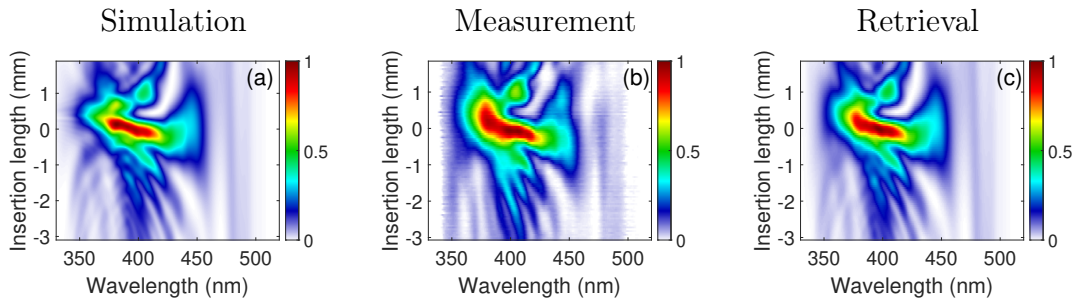

Figure 4.3: D-scan of the reference pulse.

By comparing the simulated and measured d-scan, it can already be observed that the simulation of a d-scan accurately reproduces the trace of the experimental one. Likewise, the retrieval algorithm is also able to find the correct spectral phase, since the retrieved d-scan trace looks again very similar to the measured one.

The profile of the pulse in the time domain can be obtained from the retrieval, as it is shown in Figure 4.4. According to this, the pulses used during the measurement day had a temporal width of 5.8 fs FWHM.
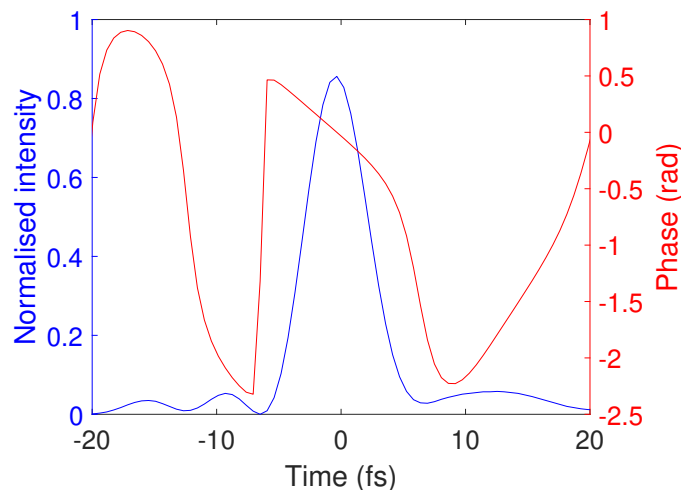

Figure 4.4: Reference pulse in the time domain.

Four d-scan measurements are made when the pulses have a time-dependent polarisation state, known in this work as the polarisation gate. The difference between

each of them is the orientation of the second polariser in the experimental setup (see Figure 3.9) so that each of the measurements corresponds to a different projection of the electric field. Figure 4.5 shows the simulated, measured and retrieved d-scan traces for each of the measurements:
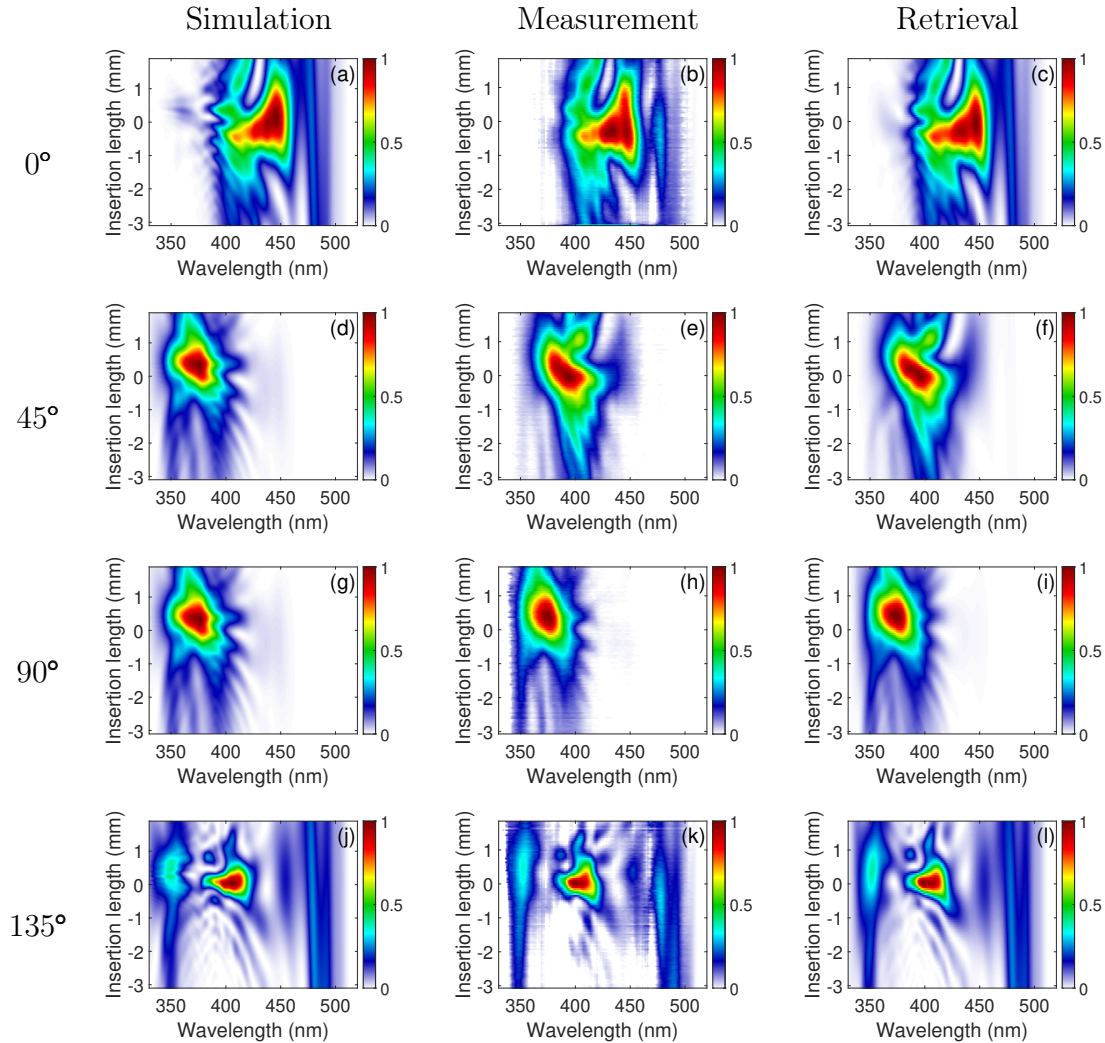

Figure 4.5: D-scan of four linearly polarised projections of the electric field. (a)-(c) 0°. (d)-(f) 45°. (g)-(i) 90°. (j)-(l) 135°.

A good agreement is observed between simulation, measurements and retrievals, which demonstrates the robustness of the simulations.

Comparing the results between the different projections, it can be seen that the spectral content varies a lot between them. This can be explained by looking at Figures 3.8 and 4.1. The second harmonic is the result of doubling the frequency of the fundamental spectrum, shown in Figure 3.8. Therefore, only the wavelengths contained in this window can contribute to the generation of the second harmonic signal. Also, each of the measurements shown in Figure 4.5 corresponds to a different projection of the electric field. As seen in Figure 4.1, the intensity distribution of the fundamental spectrum after the polariser clearly depends on its orientation. In other words, since different wavelengths of the spectrum are associated with different

polarisation states (see Figure 4.2), different projections made with the polariser result in different parts of the spectrum being cut off.

4.3   Reconstruction of the Electric Field

The retrieval algorithm obtains the spectral phase for each of the four linearly polarised projections of the electric field. Knowing the spectrum and the spectral phase one can calculate the profile of the pulse in the time domain via the Fourier transform. Figure 4.6 shows the calculated envelope of the pulse in the time domain in the transform-limited case for the four projections of the electric field.

In subsection 3.1.1 a method was detailed to generate a polarisation gate, in which the pulse becomes left circularly polarised in the front, linearly polarised in the middle with an orientation of 45° and right circularly polarised in the back. In that case, the exact position of the fast and slow axes on each waveplate was specified, allowing exact determination of the polarisation state after the wave plates. In experiments, however, it is not known which of the principal axes is which, that is, the fast and slow axes are indistinguishable. As a consequence of this, it is not possible to determine whether the polarisation in the middle of the pulse will be 45° or 135° and if the polarisation in the front and back of the pulse will be RCP and LCP or vice versa. In either case, one of the envelopes, either at 45° or 135°, should exhibit an intensity drop in the center of the pulse indicating what it is the polarisation of the middle of the pulse.

As seen in Figure 4.6b, the electric field envelope at 135° exhibits a double-peaked structure, meaning that the pulse is linearly polarised at 45°. This is a good indication that the d-scan is sensitive to variation of the polarisation state over time. The results obtained for the projections at 0°, 45° and 90° show pulse envelopes with a single peak whose width is similar to that of the input pulse. The reason is that neither of these projections is orthogonal to the pulse polarisation at any time, resulting in a pulse envelope with lower intensity but similar shape to the input.
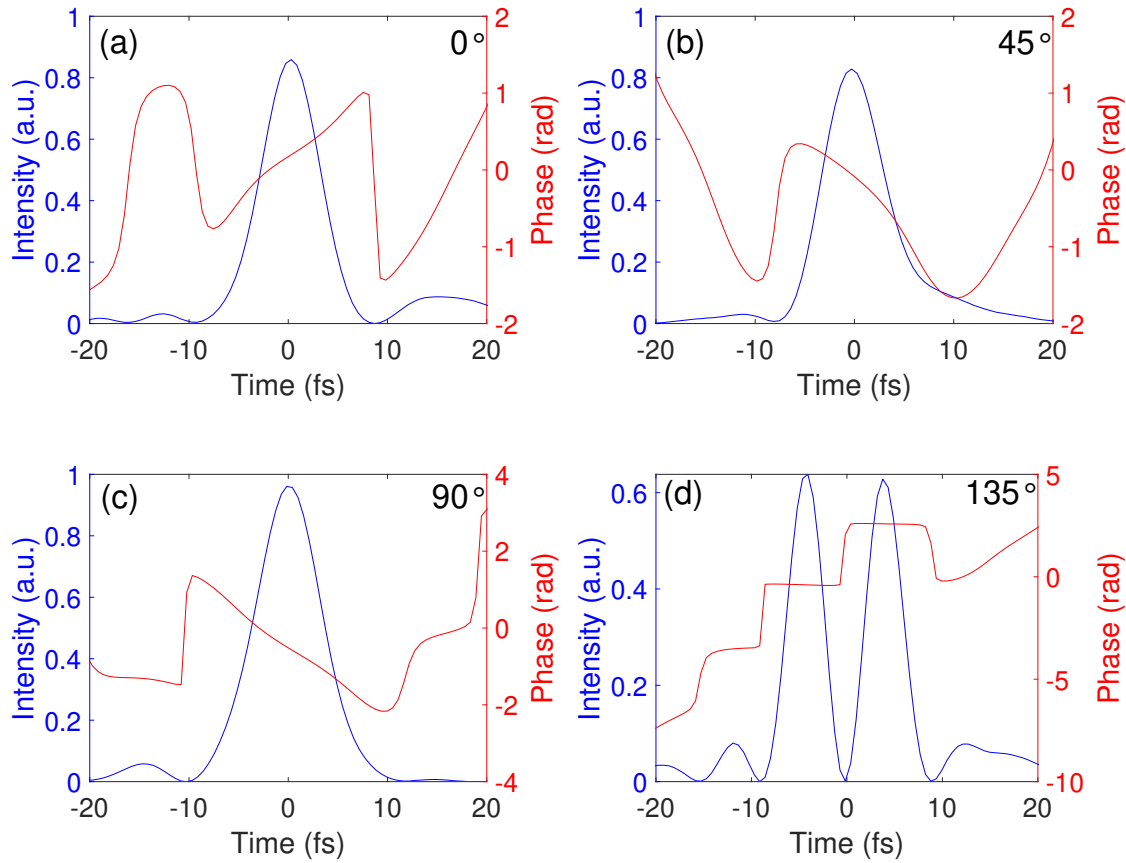
Figure 4.6: Reconstruction from retrievals of four linearly polarised projections of the pulse envelope in the time domain. (a) 0°. (b) 45°. (c). 90°. (d) 135°.

The objective of this work is to reconstruct the total electric field. As shown in Equation 2.2, this can be calculated as the sum of the complex amplitude of the electric field in two orthogonal directions. These could be, for example, the projections at 0° and 90°.

Figure 4.7a shows the calculated electric field for the projections at 0° and 90°. Figure 4.7b shows the envelope of the total electric field that results from squaring the sum of the two projections. In principle, the sum of the electric fields at 0° and 90° should reproduce the electric field at 135° since the latter can be calculated as the superposition of the other two. As seen in Figure 4.7b, this is clearly not the case since the envelope resulting from this calculation does not give the experimental result obtained after measuring the projection of the electric field at 135°, shown in Figure 4.6b. There is a good reason behind this disagreement. As noted during subsection 2.3.3, d-scan is insensitive to absolute phase and time delay. To calculate the total electric field, knowledge of both the amplitudes in two orthogonal directions and their relative phase is needed. Therefore, the sum of the fields at 0° and 90° will not give the correct result for the field a 135° since it does not consider the relative phase.

Fortunately, the relative phase between two orthogonal projections can be calculated from a third projection, for example the 135° one. To do so, the electric field

at 90° is multiplied by a phase factor until the envelope of the sum matches the experimental result obtained at 135°. Good agreement is found when multiplying by a phase factor of $\exp(-i\,1.96\pi)$, as shown in Figure 4.7d. This phase factor is specific to each measurement and cannot be determined from the setup. Its origin lies fundamentally in the insensitivity of the d-scan to time delay.
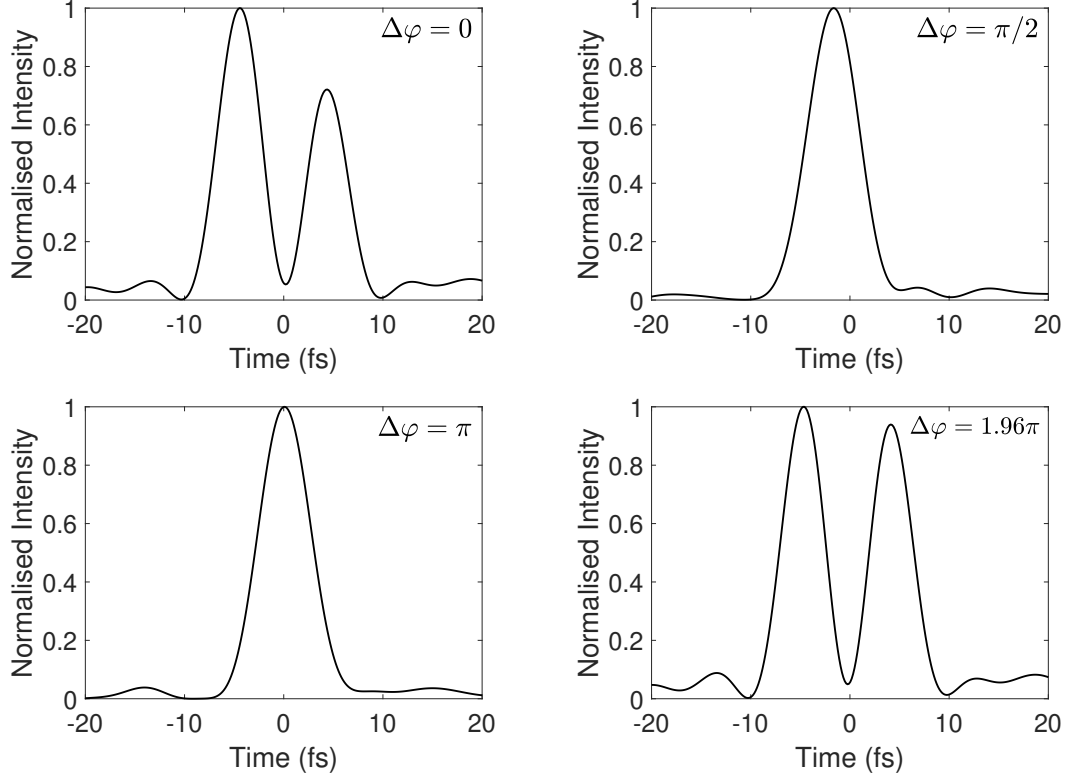

Figure 4.7: Calculation of the envelope at 135° calculated as $I_{135}(t) = |E_0(t) - E_{90}(t)\exp(i\Delta\varphi)|^2$ (a) $\Delta\varphi = 0$. (a) $\Delta\varphi = \pi/2$. (a) $\Delta\varphi = \pi$. (a) $\Delta\varphi = 1.96\pi$.

Now all the elements necessary to determine the total electric field are known. An expression for this is shown in Equation 4.1:

$$\mathbf{E}(t) = E_0(t)\,\hat{\mathbf{x}} + e^{i\,1.96\pi}E_{90}(t)\,\hat{\mathbf{y}} \tag{4.1}$$

The pulse envelope, calculated as:

$$I(t) = |E_0(t)|^2 + |E_{90}(t)|^2 \tag{4.2}$$

and the angle of ellipticity, calculated using Equation 2.15 are plotted In Figure 4.8. The simulation uses the spectrum of the input laser together with retrieved phase of the d-scan of the input laser. Comparing the results of the simulation and the experiment, it can be seen that the simulated pulse is slightly wider than the measured one. In addition to this, the ellipticity of the measured pulse is reversed compared to the simulated one. The reason for this is that it is not possible to identify which axis of the wave plates is the fast and which is the slow. This makes it impossible to predict the measurement with complete certainty.
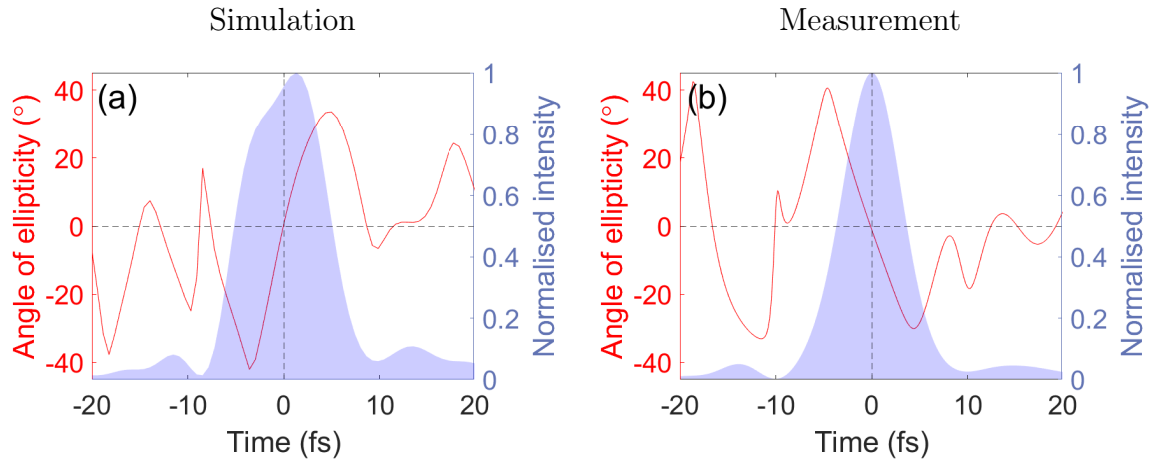
Figure 4.8: (a) Simulation of the envelope and ellipticity of the polarisation gate pulse. (b) Reconstruction from the measurements of the envelope and ellipticity of the polarisation gate pulse.

Finally, Figure 4.9 shows a three-dimensional representation of the measured electric field, where the color of the line indicates the angle of ellipticity, which can be simply observed by looking at the direction of oscillation of the electric field. Initially (negative time), the pulse is right circularly polarised, in the middle it is linearly polarised at about 45°, and in the end (positive time) it is left circularly polarised.

Figure 4.9: Reconstruction of the polarisation gate electric field. The line on the ground represents the projection of the electric field at 0° whereas the line in the background represents the projection of the electric field at 90° multiplied by the phase factor. The colored line in the middle of the image represents the total electric field, calculated as the sum of the two projections.

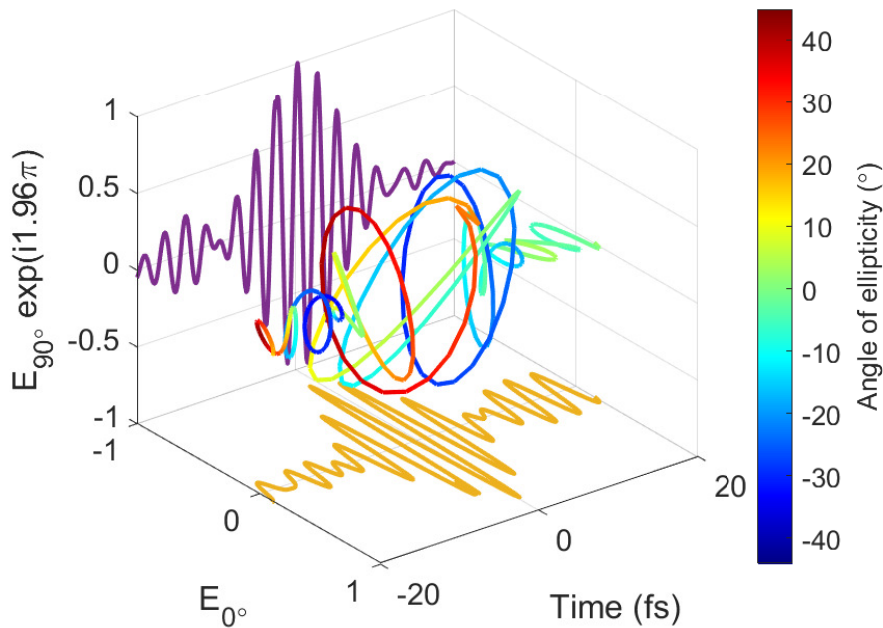# Chapter 5

Conclusion and Outlook

The results of this work have shown that to reconstruct a pulse with a time-dependent polarisation state, it is sufficient to measure the temporal characteristics of three linearly polarised projections of the electric field with the d-scan technique. The method used to generate pulses with a specific time-dependent polarisation state known as a polarisation gate was straight forward. It consisted of transmitting linearly polarised pulses through a combination of two quarter-wave plates of different order. The results have served to characterise this special polarisation state, which is commonly used in the field of attosecond science. One can calculate the polarisation gate knowing the pulse and the wave plate, but measuring it in the time domain is something totally different.

In parallel to the laboratory work, a complete framework has been developed in MATLAB to simulate and analyse the measurement of a polarisation d-scan. The modelling of polarisation and dispersion has been done using Jones matrices and vectors. A remarkable feature of the script is that it allows to include any pulse shape, wave plate and material characteristics. The ultimate goal was to simulate the polarisation d-scan as accurately as possible to obtain a d-scan trace that resembled the measurement for a given projection of the electric field. The final results have demonstrated the robustness of the simulations since the simulated and measured d-scan traces are practically indistinguishable.

In a continuation of this project, the polarisation d-scan measurement is intended to be upgraded to a single-shot configuration, for the following reason. Recording a d-scan trace can take up to a few tens of seconds, depending on the repetition rate of the laser. The realisation of the polarisation d-scan increases this time even more since three different projections must be measured. Because of this, this method only provides reliable measurements when there is sufficient pulse-to-pulse stability. Two different single-shot d-scan approaches have already been demonstrated to measure scalar pulses [34], i.e. with constant linear polarisation over time. Both include an imaging spectrometer to resolve frequency in one dimension and spatial position in the other. While one of the approaches uses a prism [43, 44], the other uses a transverse SHG crystal [45]. In both cases, there is no need to scan, since different positions in space correspond to a different glass insertion, and therefore the dispersion along with the frequency will be encoded in the spectrogram. However,

these methods cannot measure the polarisation state of light and so far no design has been proposed for such a purpose. One possible idea is to place a birefringent wedge in the setup so that different points in space also correspond to a different polarisation state. A drawing of this possible setup is shown in Figure 5.1.
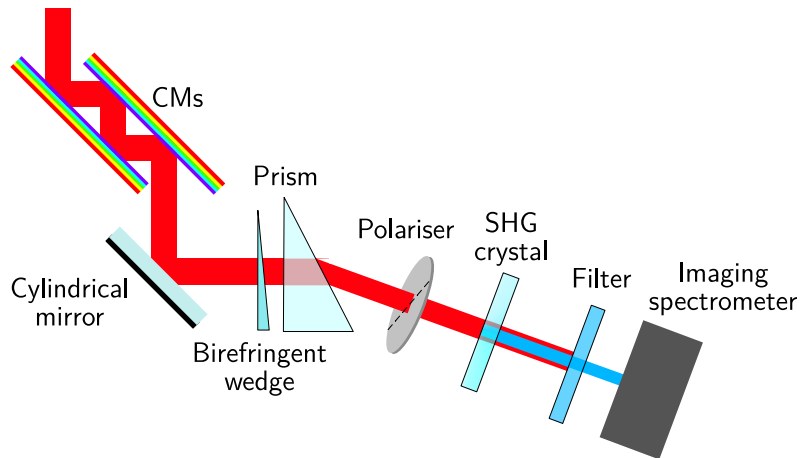
Figure 5.1: Simplified schematic of a single-shot polarisation d-scan setup.

All the elements necessary to build the single-shot polarisation d-scan setup are already in the laboratory, so it is only a matter of time before this new method can be tested.

Contribution statement

With initial supervision, I independently performed the experiments of wave plate characterisation and polarisation d-scan. I have used an existing software to obtain the d-scan retrievals. The MATLAB code for simulating polarisation d-scan was adapted from earlier scripts to include any type of material and calculate the evolution of the Jones vector through wave plates and polarisers. Other calculations, such as the wave plate characterisation analysis and polarisation gate reconstruction, were performed by me.

References

[1] Donna Strickland and Gerard Mourou. 'Compression of Amplified Chirped Optical Pulses'. In: *Optics Communications* 55.6 (1985).

[2] F. Krausz, T. Brabec and Ch. Spielmann. 'Self-starting passive mode locking'. In: *Optics Letters* 16.4 (1991).

[3] Nobuhiko Sarukura, Yuzo Ishida and Hidetoshi Nakano. 'Generation of 50-fsec pulses from a pulse-compressed, cw, passively mode-locked Ti:sapphire laser'. In: *Optics Letters* 16.3 (1991).

[4] Ahmed H. Zewail. 'Femtochemistry: Atomic-Scale Dynamics of the Chemical Bond'. In: *The Journal of Physical Chemistry* 104.24 (2011).

[5] G. Sansone et al. 'Electron localization following attosecond molecular photoionization'. In: *Nature* 465 (2010).

[6] O. Lundh et al. 'Few femtosecond, few kiloampere electron bunch produced by a laser–plasma accelerator'. In: *Nature Physics* 7 (2011).

[7] Tibor Juhasz et al. 'Corneal Refractive Surgery with Femtosecond Lasers'. In: *IEEE Journal of Selected Topics in Quantum Electronics* 5.4 (1999).

[8] K. M. Tanvir Ahmmed, Colin Grambow and Anne-Marie Kietzig. 'Fabrication of Micro/Nano Structures on Metals by Femtosecond Laser Micromachining'. In: *Micromachines* 5 (2014).

[9] Kenneth L. Sala, Geraldine A. Kenney-Wallace and Gregory E. Hall. 'CW Autocorrelation Measurements of Picosecond Laser Pulses'. In: *IEEE Journal of Selected Topics in Quantum Electronics* 16.9 (1980).

[10] Rick Trebino and Daniel J. Kane. 'Using phase retrieval to measure the intensity and phase of ultrashort pulses: frequency-resolved optical gating'. In: *Journal of Optical Society of America A* 10.5 (1993).

[11] Chris Iaconis and Ian A. Walmsley. 'Self-Referencing Spectral Interferometry for Measuring Ultrashort Optical Pulses'. In: *IEEE Journal of Selected Topics in Quantum Electronics* 35.4 (1999).

[12] Miguel Miranda et al. 'Simultaneous compression and characterization of ultrashort laser pulses using chirped mirrors and glass wedges'. In: *Optics Express* 20.1 (2011).

[13] Lina Xu et al. 'Analysis of the measurement of polarization-shaped ultrashort laser pulses by tomographic ultrafast retrieval of transverse light E fields'. In: *Journal of the Optical Society of America B* 26 (2009).

[14]   Gil Ilan Haham et al. 'V-FROG-single-scan vectorial FROG'. In: *Journal of Physics: Photonics* 3 (2021).

[15]   Benjamín Alonso and Íñigo Sola. 'Measurement of Ultrashort Vector Pulses From Polarization Gates by In-Line, Single-Channel Spectral Interferometry'. In: *IEEE Journal of Selected Topics in Quantum Electronics* 25.4 (2019).

[16]   Carlos Hernández-García et al. 'Extreme ultraviolet vector beams driven by infrared lasers'. In: *Optica* 4 (2017).

[17]   Fanqi Kong et al. 'Generating few-cycle radially polarized pulses'. In: *Optica* 6 (2019).

[18]   O. Tcherbakoff et al. 'Time-gated high-order harmonic generation'. In: *Physical Review A* 68 (2003).

[19]   Benjamín Alonso et al. 'Complete spatiotemporal and polarization characterization of ultrafast vector beams'. In: *Communications Physics* 3.151 (2020).

[20]   Carlo Altucci et al. 'Frequency-resolved time-gated high-order harmonics'. In: *Physical Review A* 58 (1998).

[21]   G. Sansone et al. 'Isolated Single-Cycle Attosecond Pulses'. In: *Science reports* 314 (2006).

[22]   I. J. sola et al. 'Controlling attosecond electron dynamics by phase-stabilized polarization gating'. In: *Nature Physics* 2 (2006).

[23]   A. Flettner et al. 'Ellipticity dependence of atomic and molecular high harmonic generation'. In: *The European Physical Journal D* 21 (2002).

[24]   R. Cireasa et al. 'Probing molecular chirality on a sub-femtosecond timescale'. In: *Nature Physics* 11 (2015).

[25]   David Ayuso et al. 'Synthetic chiral light for efficient control of chiral light–matter interaction'. In: *Nature Physics* 13 (2019).

[26]   G. Spektor et al. 'Revealing the subfemtosecond dynamics of orbital angular momentum in nanoplasmonic vortices'. In: *Science* 355 (2017).

[27]   A. V. Kimel et al. 'Ultrafast non-thermal control of magnetization by instantaneous photomagnetic pulses'. In: *Nature* 435 (2005).

[28]   A. E. Paul et al. 'Time-resolved measurements of the polarization state of four-wave mixing signals from GaAs multiple quantum wells'. In: *Journal of the Optical Society of America B* 13 (1996).

[29]   W. J. Walecki et al. 'Characterization of the polarization state of weak ultrashort coherent signals by dual-channel spectral interferometry'. In: *Optics Letters* 22 (1997).

[30]   L. Lepetit G. Chériaux and M. Joffre. 'Linear techniques of phase measurement by femtosecond spectral interferometry for applications in spectroscopy'. In: *Journal of the Optical Society of America B* 12 (1995).

[31]   Bahaa E.A Saleh and Malvin C. Teich. *Fundamentals of Photonics*. Wiley Series, 2019.

[32]   Eugene Hecht. *Optics*. 5th ed. Pearson, 2017.

[33] Herman A. Haus. 'Mode-Locking of Lasers'. In: *IEE Journal on Selected Topics in Quantum Electronics* 6.6 (2000).

[34] Ivan Sytecevich et al. 'Characterizing ultrashort laser pulses with second harmonic dispersion scans'. In: *Journal of the Optical Society of America B* 38.5 (2021).

[35] Ian Walmsley, Leon Waxer and Christophe Dorrer. 'The role of dispersion in ultrafast optics'. In: *Review of Scientific Instruments* 72.1 (2001).

[36] Miguel Miranda et al. 'Simultaneous compression and characterization of ultrashort laser pulses using chirped mirrors and glass wedges'. In: *Optics Express* 20 (2012).

[37] Miguel Miranda et al. 'Characterization of broadband few-cycle laser pulses with the d-scan technique'. In: *Optics Express* 20 (2012).

[38] Esmerando Escoto et al. 'Advanced phase retrieval for dispersion scan: a comparative study'. In: *Journal of the Optical Society of America B* 35 (2018).

[39] Miguel Miranda et al. 'Fast iterative retrieval algorithm for ultrashort pulse characterization using dispersion scans'. In: *Journal of the Optical Society of America B* 34 (2017).

[40] Benjamín Alonso, Iñigo J. Sola and Helder Crespo. 'Self-calibrating d-scan: measuring ultrashort laser pulses on-target using an arbitrary pulse compressor'. In: *Scientific Reports* 8 (2018).

[41] Neven Ibrakovic et al. 'Achromatic dual-waveplate for inline two color high-order harmonic generation'. In: *The European Physical Journal D* 72.148 (2018).

[42] Anne Harth et al. 'Compact 200kHz HHG source driven by a few-cycle OP-CPA'. In: *Journal of Optics* 20.1 (2018).

[43] D. Fabris et al. 'Single-shot implementation of dispersion-scan for the characterization of ultrashort laser pulses'. In: *Optics Express* 23 (2015).

[44] Maïté Louisy et al. 'Compact single-shot d-scan setup for the characterization of few-cycle laser pulses'. In: *Applied Optics* 56 (2017).

[45] F. J. Salgado-Remacha et al. 'Single-shot d-scan technique for ultrashort laser pulse characterization using transverse second-harmonic generation in random nonlinear crystals'. In: *Applied Optics* 56 (2017).

Appendix A

MATLAB Scripts

Below is an example of the MATLAB code used to simulate the measurement of a polarisation d-scan:

```matlab
% Simulation of polarisation d-scan

%% Constants

% Speed of light in vacuum m/s
c0 = 299792458;

%% Select parameters for the simulation

% Number of frequency points
N1 = 2^14;

% Number of points for Fast Fourier Transformation (FFT)
N2=2^16;

% Input pulse duration (fs)
tau = 6;

% Frequency array (PHz)
f0=linspace(0.25,1,N1);
f=permute(f0,[1,3,2]);
f_central=f0(1)+(f0(end)-f0(1))/2; % central frequency

% Wavelength (um)
wl=0.3./f0;

% Wavenumber (um-1)
k=2*pi./wl;

% Angular frequency (rad*PHz)
w0=2*pi*f0;

% Material insertion array from the wedges (m)
l=linspace(-2e-3,3e-3,201)';

%thickness zero-order quarter wave plate (um)
```

```matlab
37   L0=22.4856;
38
39   %% Import refractive index from Sellmeier equations
40
41   % BK7 refractive index
42   n_BK7=nBK7(f0*1e15);
43
44   % Quartz ordinary refractive index
45   no=qzo(wl);
46
47   % Quartz extraordinary refractive index
48   ne=qze(wl);
49
50   %% Define Jones matrices of optical elements
51
52   % Rotation matrices for 45 degree frame rotation
53   R1=[cos(pi/4),sin(pi/4);-sin(pi/4),cos(pi/4)];
54   R2=[cos(pi/4),-sin(pi/4);sin(pi/4),cos(pi/4)];
55
56   % Zero-order quarter-wave plate (QW0)
57   M1=zeros(2,2,N1);
58   M1(1,1,:)=exp(0*k); %1
59   M1(2,2,:)=exp(1i*k.*(ne-no)*L0); % wave retardence
60
61   % Third-order quarter-wave plate (QW3)
62   M2=zeros(2,2,N1);
63   M2(1,1,:)=exp(0*k);
64   M2(2,2,:)=exp(1i*7*k.*(ne-no)*L0);
65
66   %% Select input spectral amplitude
67
68   % Use Gaussian arbitrary spectrum
69
70   %amp = exp(-pi^2*tau^2*(f0-f_central).^2)';
71   %I_spectrum = abs(amp).^2;
72
73   % Import measured fundamental spectrum on 2022-03-07
74
75   data_spectrum = load('0703_0_0_gate_reference_spectrum.txt');
76
77   f_spectrum = 1e-6*c0./data_spectrum(:,1); % frequency axis in PHz
78   I_spectrum = data_spectrum(:,2).*(data_spectrum(:,1).^2)./c0; % ...
         the wavelength spectrum is multiplied by a scaling factor to ...
         obtain the frequency spectrum
79   I_spectrum(2611:end) = 0; % set noise to zero
80
81   I_spectrum_new = ...
         interp1(flip(f_spectrum),flip(I_spectrum),f0,'spline','extrap')';
82
83   I_spectrum_new(I_spectrum_new<0)=0; % set noise to zero
84   amp=sqrt(I_spectrum_new); % convert intensity into amplitude
85
86   %% Select input spectral phase
87
88   % Use arbitrary phase
89
90   % ph2 = 0 *(f0-f_central)'.^2; %some quadratic phase around ...
         central frequency
```

```matlab
91  % ph3 = 0 *(f0-f_central)'.^3; %some 3rd order phase around ...
        central frequency
92  % phase=ph2+ph3;
93
94  % Import retrieved phase from reference d-scan: 2022-03-07
95
96  data_phase=load('0703_ref.txt');
97
98  f_phase = 1e-6*c0./data_phase(:,1); % frequency axis in PHz
99  phase_data = data_phase(:,3); % from 600 nm to 1100 nm
100
101 phase=interp1(flip(f_phase),flip(phase_data),f0,'linear','extrap')';
102
103
104 %% Resulting complex spectral amplitude of the incoming beam
105
106 amp = amp.*exp(1i*phase); % spectral amplitude and phase of the ...
        incoming pulses
107
108 %% Polarisation state of the incoming pulses before the waveplates
109
110 % Jones vector of vertically polarised light
111 v=[0;1];
112
113 %% Creating a time dependent polarisation state
114
115 % Initialisation output, wavelength vs amplitude
116 u=zeros(2,N1);
117
118 % Iteration over all wavelengths: propagation through first and ...
        second
119 % waveplate. Polarisation gate is QW3 at 45deg -- QW0 at 0deg
120
121 % The angle \theta inside rotation_matrix(\theta) selects the ...
        projection of
122 % electric field
123
124 for i=1:N1
125     %u(:,i)=rotation_matrix(0)*M1(:,:,i)*M2(:,:,i)*v; % ...
            Reference. QW3 wave plate at 0, QW0 wave plate at 0.
126     u(:,i)=rotation_matrix(0)*M1(:,:,i)*R2*M2(:,:,i)*R1*v; % ...
            Polarisation gate. QW3 wave plate at 45, QW0 wave plate ...
            at 0.
127
128 end
129
130
131 %% Propagation through  BK7 wedges
132
133 % Wavenumber in BK7
134 ke = ((1/pi)*w0*1e15/c0).*n_BK7; % m-1
135
136 ampS1 = amp.*u(1,:)'.*exp(1i*pi*ke.*l)';
137 ampS2 = amp.*u(2,:)'.*exp(1i*pi*ke.*l)';
138
139 %% Calculate Jones vector in the time domain
140
141 df=mean(diff(f)); % Frequency spacing
```

```matlab
142  t=linspace(0.5/df,-0.5/df,N2); % Corresponding time spacing
143
144  ampT1=fftshift(fft(ampS1,N2)); % Horizontal projection
145  ampT2=fftshift(fft(ampS2,N2)); % Vertical projection
146
147  %% Second harmonic generation (SHG)
148
149  % Frequency axis for second harmonic
150  fshg = df*[0:N2-1]+2*min(f0);
151
152  % Get SHG spectra: FT spectrum with multiplied phase, square it ...
         (shg is
153  % intensity dependend), then IFT it back
154  ampSHG1=ifft(fft(ampS1,N2).^2); % d-scan trace horizontal projection
155  ampSHG2=ifft(fft(ampS2,N2).^2); % d-scan trace vertical projection
156
157  % These are the spectrograms (d-scan traces) with material ...
         insertion in one axis and
158  % frequency in the other axis.
```

Below is an example of the MATLAB code used to calculate the polarisation gate pulse:

```matlab
1  %  calculation polarisation gate
2
3  %  calculation polarisation gate
4
5  %% Constants
6
7  % speed of light in vacuum (m/s)
8  c0 = 299792458;
9
10  %% Select parameters for the simulation
11
12  % Number of points in frequency array
13  N1 = 10000;
14
15  % Number of points for Fast Fourier Transform (FFT)
16  N2 = 2^16;
17
18  % Input pulse duration (fs)
19  tau = 6;
20
21  % Frequency (PHz)
22  f0=linspace(0.25,0.5,N1);
23  f=permute(f0,[1,3,2]);
24  f_central=f0(1)+(f0(end)-f0(1))/2; % central frequency
25
26  % Wavelength (um)
27  wl=0.3./f0;
28
29  % Wavenumber (um-1)
30  k=2*pi./wl;
31
32  % Angular frequency (rad*PHz)
33  w0=2*pi*f0;
```

```matlab
34
35   % Thickness zero-order quarter wave plate (um)
36   L0=22.4856;
37
38   %% Refractive index from Sellmeier equations
39
40   % Quartz ordinary refractive index
41   no=qzo(wl);
42
43   % Quartz extraordinary refractive index
44   ne=qze(wl);
45
46   %% Define Jones matrices of optical elements
47
48   % Rotation matrices for 45 degree frame rotation
49   R1=[cos(pi/4),sin(pi/4);-sin(pi/4),cos(pi/4)];
50   R2=[cos(pi/4),-sin(pi/4);sin(pi/4),cos(pi/4)];
51
52   % Zero-order quarter-wave plate (QW0)
53   M1=zeros(2,2,N1);
54   M1(1,1,:)=exp(0*k); %1
55   M1(2,2,:)=exp(1i*k.*(ne-no)*L0); % wave retardence
56
57   % Third-order quarter-wave plate (QW3)
58   M2=zeros(2,2,N1);
59   M2(1,1,:)=exp(0*k);
60   M2(2,2,:)=exp(1i*7*k.*(ne-no)*L0);
61
62   %% Select input spectral amplitude
63
64   % Use Gaussian arbitrary spectrum
65
66   amp = exp(-pi^2*tau^2*(f0-f_central).^2)';
67   I_spectrum = abs(amp).^2;
68
69   % Import measured fundamental spectrum on 2022-03-07
70
71   % data_spectrum = load('0703_0_0_gate_reference_spectrum.txt');
72   %
73   % f_spectrum = 1e-6*c0./data_spectrum(:,1); % frequency axis in PHz
74   % I_spectrum = data_spectrum(:,2).*(data_spectrum(:,1).^2)./c0; ...
         % the wavelength spectrum is multiplied by a scaling factor ...
         to obtain the frequency spectrum
75   % I_spectrum(2611:end) = 0; % set noise to zero
76   %
77   % I_spectrum_new = ...
         interp1(flip(f_spectrum),flip(I_spectrum),f0,'spline','extrap')';
78   %
79   % I_spectrum_new(I_spectrum_new<0)=0; % set noise to zero
80   % amp=sqrt(I_spectrum_new); % convert intensity into amplitude
81
82   %% Select input spectral phase
83
84   % Use arbitrary phase
85
86   ph2 = 0 *(f0-f_central)'.^2; %some quadratic phase around ...
         central frequency
87   ph3 = 0 *(f0-f_central)'.^3; %some 3rd order phase around ...
```

```matlab
         central frequency
88  phase = ph2+ph3;
89
90  % Import retrieved phase from reference d-scan: 2022-03-07
91
92  % data_phase=load('0703_ref.txt');
93  %
94  % f_phase = 1e-6*c0./data_phase(:,1); % frequency axis in PHz
95  % phase_data = data_phase(:,3); % from 600 nm to 1100 nm
96  %
97  % ...
        phase=interp1(flip(f_phase),flip(phase_data),f0,'linear','extrap')';
98
99  %% Resulting complex spectral amplitude of the incoming beam
100
101 amp = amp.*exp(1i*phase); % spectral amplitude and phase of the ...
        incoming pulses
102 I_spectrum = abs(amp).^2;
103
104 %% Calculation of the  temporal profile of the incoming pulse
105
106 df=mean(diff(f)); % Frequency spacing
107 t=linspace(0.5/df,-0.5/df,N2); % Corresponding time spacing
108
109 ampT=fftshift(fft(amp,N2));
110
111 %% Polarisation state of the incoming pulses before the waveplates
112
113 % Jones vector of vertically polarised light
114 v=[0;1];
115
116 %% Creating a time-dependent polarisation state
117
118 % Initialisation output Jones vector, wavelength vs amplitude
119 u=zeros(2,N1);
120
121 % Iteration over all wavelengths
122 for i=1:N1
123
124     u(:,i)=R1*M1(:,:,i)*R2*M2(:,:,i)*R1*v;   % Polarisation ...
            gate. QW3 wave plate at 45, QW0 wave plate at 0.
125
126 end
127
128 %% Spectral intensity after waveplate
129
130 ampS1 = amp'.*u(1,:); % Horizontal projection
131 ampS2 = amp'.*u(2,:); % Vertical projection
132
133 %% Calculation of the time-dependent Jones vector
134
135 df=mean(diff(f)); % Frequency spacing (PHz)
136 t=linspace(0.5/df,-0.5/df,N2); % Corresponding time spacing (fs)
137
138 ampT1=fftshift(fft(ampS1,N2)); % Horizontal projection
139 ampT2=fftshift(fft(ampS2,N2)); % Vertical projection
140
141 % Time-dependent Jones vector
```

```matlab
142  u_t=[ampT1;ampT2];
143
144  %% Calculation of amplitude ratio, relative phase and ellipticity
145
146  % Amplitude ratio
147  ampRatio=abs(u_t(2,:))./abs(u_t(1,:));
148
149  % Relative phase
150  relPhase=angle(u_t(2,:))-angle(u_t(1,:));
151
152  % Ellipticity from amplitude ratio and relative phase
153  chi=(1/2)*asin((2*ampRatio./(1+ampRatio.^2)).*sin(relPhase)); % ...
         ellipticity angle (rad)
154  chi=chi*(180/pi); % ellipticity angle (degrees)
155
156  %% Intensity envelope of the polarisation gate
157
158  iT_new = abs(u_t(1,:)).^2 + abs(u_t(2,:)).^2;
```

Below is an example of the MATLAB code used to simulate the wave plate characterisation measurements:

```matlab
 1  % simulation of wave plate characterisation
 2
 3  %% Constants
 4
 5  % speed of light in vacuum (m/s)
 6  c0 = 299792458;
 7
 8  %% Select parameters for the simulation
 9
10  %number of frequency points
11  N1 = 2048;
12
13  % Input pulse duration (fs)
14  tau = 6;
15
16  % Frequency (PHz)
17  f0=linspace(0.25,0.5,N1);
18  f=permute(f0,[1,3,2]);
19  f_central=f0(1)+(f0(end)-f0(1))/2; % central frequency
20
21  % Wavelength (um)
22  wl=0.3./f0;
23  wl_new = linspace(0.5,1.1,N1); % for interpolation
24
25  % Wavenumber (um-1)
26  k=2*pi./wl;
27
28  % Angular frequency (rad*PHz)
29  w0=2*pi*f0;
30
31  % Thickness zero-order quarter wave plate (um)
32  L0=22.4856;
33
34  %% Refractive index from Sellmeier equations
```

```matlab
35
36  % Quartz ordinary refractive index
37  no=qzo(wl);
38
39  % Quartz extraordinary refractive index
40  ne=qze(wl);
41
42  %% Define Jones matrices of optical elements
43
44  % Rotation matrices for 45 degree frame rotation
45  R1=[cos(pi/4),sin(pi/4);-sin(pi/4),cos(pi/4)];
46  R2=[cos(pi/4),-sin(pi/4);sin(pi/4),cos(pi/4)];
47
48  % Zero-order quarter-wave plate (QW0)
49  M1=zeros(2,2,N1);
50  M1(1,1,:)=exp(0*k); %1
51  M1(2,2,:)=exp(1i*k.*(ne-no)*L0); % wave retardence
52
53  % Third-order quarter-wave plate (QW3)
54  M2=zeros(2,2,N1);
55  M2(1,1,:)=exp(0*k);
56  M2(2,2,:)=exp(1i*7*k.*(ne-no)*L0);
57
58  %% Select input spectral amplitude
59
60  % Use Gaussian arbitrary spectrum
61
62  amp = exp(-pi^2*tau^2*(f0-f_central).^2)';
63  I_spectrum = abs(amp).^2;
64
65  %% Select input spectral phase
66
67  % Use arbitrary phase
68
69  ph2 = 0 *(f0-f_central)'.^2; %some quadratic phase around ...
        central frequency
70  ph3 = 0 *(f0-f_central)'.^3; %some 3rd order phase around ...
        central frequency
71  phase = ph2+ph3;
72
73  %% Resulting complex spectral amplitude of the incoming beam
74
75  amp = amp.*exp(1i*phase); % spectral amplitude and phase of the ...
        incoming pulses
76  I_spectrum = abs(amp).^2;
77
78  %% Normalise spectrum
79
80  I_spectrum_norm=I_spectrum.*0+1;
81  amp_norm=amp.*0+1;
82
83  I_spectrum_norm=interp1(flip(wl),flip(I_spectrum_norm),wl_new,'spline');
84  amp_norm=interp1(flip(wl),flip(amp_norm),wl_new,'spline');
85
86  %% Polarisation state of the incoming pulses before the waveplates
87
88  % Jones vector of vertically polarised light
89  v=[0;1];
```

```matlab
90
91   %% Evolution of the Jones vector through the wave plates
92
93
94   wl = flip(wl);
95
96   % Initialisation output, wavelength vs amplitude
97   u=zeros(2,N1,18);
98
99   % Iteration over 19 projections
100  theta=linspace(0,170,18);
101  theta_rad=theta.*(pi/180);
102
103  % Iteration over all analyser projections
104  for j=1:18
105
106      R=rotation_matrix(theta_rad(j));
107
108      % iteration over all wavelengths
109      for i=1:N1
110
111          u(:,i,j)=R*R2*M1(:,:,i)*R1*v; % QW0 at 45 degrees
112          %u(:,i,j)=R*R2*M2(:,:,i)*R1*v; % QW3 at 45 degrees
113          %u(:,i,j)=R*M1(:,:,i)*R2*M2(:,:,i)*R1*v; % Polarisation ...
                  gate. QW3
114          %at 45 degrees and QW0 at 0 degrees
115
116      end
117
118  end
119
120
121
122  %% Spectral intensity after waveplate
123
124  ampS1_norm=amp_norm.*u(1,:,:);
125  ampS2_norm=amp_norm.*u(2,:,:);
126
127  S1_norm=squeeze(ampS1_norm);
128  S2_norm=squeeze(ampS2_norm);
129
130  %%  Define fit parameters
131
132  lambdai = 0.620; % start wavelength
133  lambdaf = 0.900; % end wavelength
134
135  N = 20; % number of wavelengths to fit
136  step = (lambdaf-lambdai)/(N-1); % spacing between fitted wavelengths
137  lambda1 = lambdai + step;
138
139  [minval,lambdai_ind]=min(abs(wl_new-lambdai));
140  [minval,lambda1_ind]=min(abs(wl_new-lambda1));
141  step=lambda1_ind-lambdai_ind;
142
143
144  %% Fit each wavelength data to an oscillating function and ...
         calculate Stokes paramters from it
145
```

```matlab
146  % Initialise lists to store the calculated Stokes parameters
147  s0=[];
148  s1=[];
149  s2=[];
150  s3=[];
151
152  array_theta = linspace(0,170*pi/180,1e5);
153
154  for n = 1:N
155      myfittype = fittype('a + ...
             b*cos(x+c)^2','dependent',{'y'},'independent',{'x'},'coefficients',{'a','b'
156      myfit = ...
             fit(theta_rad(:),abs(S1_norm(lambdai_ind+step*(n-1),:)).^2',myfittype);
157
158      % Calculate parameters of the polarisation ellipse
159      Imax=myfit.a+myfit.b;
160      Imin=myfit.a;
161      chi=atan(sqrt(Imin/Imax));
162      Ix=myfit.a+myfit.b*cos(0+myfit.c)^2;
163      Iy=myfit.a+myfit.b*cos(pi/2+myfit.c)^2;
164      R=sqrt(Ix/Iy);
165      phi=asin(((1+R^2)/(2*R))*sin(2*chi));
166
167      % Calculate Stokes parameters
168      s0_val=Ix+Iy;
169      s1_val=Ix-Iy;
170      s2_val=2*sqrt(Ix)*sqrt(Iy)*cos(phi);
171      s3_val=2*sqrt(Ix)*sqrt(Iy)*sin(phi);
172
173      s0(n)=s0_val;
174      s1(n)=s1_val;
175      s2(n)=s2_val;
176      s3(n)=s3_val;
177
178  end
```